Wisam Ali Mohamad Issa

Analysis of the voltage-reactive power control mode impact on photovoltaic systems energy generation curtailment

Campo Grande - Mato Grosso do Sul

August, 2023

Wisam Ali Mohamad Issa

Analysis of the voltage-reactive power control mode impact on photovoltaic systems energy generation curtailment

Work presented in order to partially fulfill the necessary requirements to achieve the master degree in Electrical Engineering granted by the Federal University of Mato Grosso do Sul - Brazil

Federal University of Mato Grosso do Sul

College of Engineerings, Architecture and Urbanism and Geography

Electrical Engineering Graduate Program

Supervisor: Dr. Luigi Galotto Junior

Campo Grande - Mato Grosso do Sul

August, 2023

Wisam Ali Mohamad Issa

Analysis of the voltage-reactive power control mode impact on photovoltaic systems energy generation curtailment

Work presented in order to partially fulfill the necessary requirements to achieve the master degree in Electrical Engineering granted by the Federal University of Mato Grosso do Sul - Brazil

Work approved in September 07, 2023.

Dr. Luigi Galotto Junior
Advisor

Dr. João Onofre Pinto
Internal Titular

Dr. Leon Tolbert
External Titular

Campo Grande - Mato Grosso do Sul

August, 2023

ACKNOWLEDGEMENTS

Certainly, there are many people which contributed in a significant way to the development of this work. To make an exhaustive list containing all of their names is a hard task. However, it would be unfair to not mention some of the most influential professionals whose names should be on it.

First of all, I want to thank my academic advisor, Dr. Luigi Galotto, for his valuable discussions surrounding several challenges which I faced while developing this work.

Secondly, I want to thank Dr. João Onofre for providing many useful insights pertaining to the scope of this work through all of our discussions.

At last, but not least, it is also important to thank Dr. Leon Tolbert, which not only provided me the enriching opportunity of working on the topic of this work at the University of Tennessee, but also, through his suggestions, made possible for me to, in a great extent, improve the results of my work.

RESUMO

Este trabalho possui como tema principal o estudo da redução do aproveitamento de sistemas fotovoltaicos interligados à rede na produção de energia elétrica devido ao emprego do algoritmo de controle tensão-potência reativa, popularmente denominado volt-var, quando a potência reativa resultante da aplicação dele é priorizada em contrapartida à potência ativa feita disponível para conversão pelos painéis fotovoltaicos. Mais especificamente, almejou-se como objetivo principal o estudo da sensibilidade da limitação de conversão de energia elétrica perante parâmetros das linhas dos sistemas, as diferenças sazonais entre a demanda de cargas e a disponibilidade de irradiação solar, a influência de dispositivos de regulação de tensão da operadora do sistema (bancos de capacitores e reguladores de tensão em transformadores), assim como a intensificação da participação de sistemas fotovoltaicos na rede.

Para alcançar esses objetivos, foram executadas diversas simulações em três alimentadores disponibilizados na literatura. Após a exibição dos resultados, foi possível constatar, dentre outras conclusões, que quando a penetração de geradores solares distribuídos é baixa, os esforços realizados por seus inversores para a mitigação de desvios de tensão da rede possuem relação mais forte com condições intrínsecas à rede do que com a própria geração deles, embora o contrário tenha sido verificado quando o nível de penetração é alto.

A sazonalidade das curvas de demanda das cargas e de irradiação solar permitiram observar diferenças importantes nas estações em que os piores casos de redução de geração ocorreram, que também dependem do nível de penetração dos sistemas fotovoltaicos na rede.

Verificou-se também que até mesmo em sistemas elétricos considerados fortes é possível que ocorra uma redução alta na produção de energia elétrica caso o carregamento neles seja alto e o nível de penetração de seus sistemas fotovoltaicos seja baixo.

Por sua vez, o nível de penetração em si é um fator importante, especialmente para redes fracas cujas porcentagens de redução na geração de energia dependem mais intensamente dessa variável.

Por fim, embora reguladores de tensão tenham demonstrado impacto predominantemente positivo na redução do esforço necessário pelas unidades de geração distribuída para a regulação de tensão, e, consequentemente, tenham contribuído para mitigar a redução de produção de energia delas, foi possível identificar situações em que, devido ao fato desses dispositivos afetarem a regulação de tensão de partes do sistema de distribuição apenas, a redução do esforço despendido pelas unidades geradoras localizadas nessas regiões contribuiu de forma significativa para o aumento do esforço por outras localizadas fora delas.

ABSTRACT

This work has as its main theme the study of the reduction of grid-connected photovoltaic systems energy production employing voltage-reactive power control due to the prioritization of the reactive power output requested by the algorithm. More specifically, the intended main objective was to study the sensitivity of this curtailment phenomenon relative to the power system line parameters (resistances and inductances), the seasonal variances of the loads demand curves and solar irradiance timeseries, the influence of the electric power system (EPS) voltage regulation devices such as capacitor banks and transformers with tap changers, as well as the intensification of the participation of photovoltaic systems within the EPS.

In order to attain the proposed objective, several simulations were executed in three different feeders available in the literature. Based on the results, it was possible to verify, among other conclusions, that when the penetration level of solar distributed generators is low, the efforts of their inverters are more strongly related to the mitigation of voltage regulation issues resulting from the grid own conditions, rather than their own generation.

The seasonal characteristic of the loads demand curves, as well as the solar irradiation allowed to observe important differences in the season of the year in which the worst curtailment occurred, which also depend on the penetration level of the photovoltaic systems within the grid.

It was also verified that even strong grids can present high relative curtailments if they are heavily loaded and the penetration level of the photovoltaic systems within them is low.

The influence of the penetration level itself is an important factor, specially if the feeder is weak, a case for which it was verified that the overall curtailment depends more strongly on this variable.

Finally, although tap changers demonstrated to predominantly impact positively the required effort from the distributed generation units for voltage support, since they only affect a part of the system, other units located outside of this region may have to sacrifice more their own generation in order to comply with the volt-var, due to the lack of contribution from the inverters located on the mentioned affected section.

LIST OF FIGURES

LIST OF TABLES

CONTENTS

1 INTRODUCTION

Electrical energy is, undoubtedly, one of the key elements that allowed humanity to progress its societies through the last century. Stating its importance does not need justification. Traditionally, it was produced in concentrated regions, normally not close to the consumers. In order to make possible electricity generation far away from where it is consumed, these two regions need to be linked through a transmission system which, in the consumption end, is connected to another system with a lower voltage level, known as distribution network [1], that exist as a mean to make the produced energy available to its consumers.

It is reasonable to think that the energy delivered by the distribution system must maintain a proper level of quality in order to not negatively impact its loads. In fact, it is required of them to operate within restricted limits and standards [1]. Deviations of the defined properties can result in reduction of efficiency, reduced expectation of consumers assets lifetimes or even damages to them [2].

The level of quality mentioned before is a function of not only the electrical power system (EPS) assets, such as cables, transformers, etc., but also of the consumers loads [2]. Therefore, the EPS operator should not be considered as the solely responsible for maintaining power quality. This consideration is important in order to understand the regulation policies which are applied to consumers.

The traditional model of the EPS, presenting only unidirectional power flow (with the roles of consumers well defined), as described previously, is challenged by the proliferation of distributed energy resources (DERs), such as photovoltaic systems (PVs), due to several reasons [3, 4, 5, 6, 7]. The most prominent of them, in frequency domain, may be their ability to cause an undesired rise of voltage across the distribution system.

As a countermeasure, standards such as IEEE 1547-2018 [8], aiming to regulate the minimum capabilities that inverters for distributed energy resource applications should have, specify that they should be able to operate in different modes respecting certain criteria, with the intent of providing support to the grid or mitigating their possible negative effects.

Within IEEE 1547, one of these modes, pertaining to voltage regulation in steady-state operation, is the voltage-reactive power control, also known as volt-var. Inverters operating in this condition have to inject reactive power following a piece-wise linear function based on the average value of the effective voltages measured at the inverter point of common coupling (PCC) with the EPS. Although several studies suggest the effectiveness of this strategy in mitigation of undesired voltage profile rises [3, 9, 10, 11], there is not sufficient data about the effect of using this algorithm in the curtailment of energy production from distributed units, since, during periods of peak generation, they may have to curtain part of their available active power in order to prioritize the reactive

power demanded by the control mode.

Hence, this work tries to assess the impact on the curtailment of energy generation, in medium-voltage distribution systems, of the employment of the volt-var algorithm.

1.1 Motivation of this work

The volt-var algorithm is simple to implement, specially because it does not require communication with other assets in the distribution level. This observation, in combination with the efficacy of the algorithm, as mentioned previously, is sufficient to justify its popularity in the literature.

The impact of methods that may curtain energy production favoring reactive power injection, for voltage support, were considered before in existing works. In [12], for example, the employment of a power conditioning system (PCS) on a feeder with a high number of installed inverters was observed and the generation loss due to the active power curtailment caused by its operation was estimated, albeit the algorithm that the device was specified to employ can be seen as a combination of the constant power factor with the voltage-active power modes of the 1547 standard, and, hence, it is significantly different from volt-var. Also, some of the generation units which the data used in the study is based from contained energy storage systems, which can significantly reduce the necessary curtailment of active power generation.

On the other hand, [13] exhibits results from an almost equivalent problem in comparison with the previous work, and, hence, can be considered in the same manner.

Also, [14] contributed in evaluating similar propositions, accounting for inverters tripping due to severe high voltage. This study, however, concentrated on a comparison between the performance of different control modes for voltage support during steady-state, rather than an analysis of the volt-var curtailment nature by itself.

All of the previous works concluded that there is a reasonable, albeit variable, loss of generation associated with the class of frequency-domain voltage-support methods that use reactive power. However, the commented analyses either were executed with a different algorithm (not volt-var), did not considered how the results may change through the different seasons of an year or employed low-voltage feeders, in which the referred group of methods, including volt-var, is less efficient. Also, in the low-voltage side of the distribution system (after the transformer), it is not usual to exist tap changers or capacitor banks, and, hence, an analysis of the effect of those devices on the energy curtailment could not be identified.

Therefore, it still remains as an open question how much, in the medium-voltage level of a distribution system, should volt-var impact its DERs energy production. Considering the discussion in this work introduction, it is also important to evaluate what are the factors

of an EPS which can influence this assessment. Maybe the most relevant question would be if significant active power curtailment can occur in situations that can be considered as not a liability of the generation units.

The previous statements are the questions motivating this work. Emphasis has been given for the case of PV systems as the DERs.

1.2 Objective of this work

1.2.1 General objective

Evaluate the impact of the volt-var algorithm, in medium-voltage electrical grids, on the energy production curtailment of photovoltaic-based systems.

1.2.2 Specific objectives

- Analyze the differences between reductions in photovoltaic system units energy generation, complying with voltage-reactive power control, as their penetration level increases within distribution systems;
- Assess the influence of the feeder strength and identify other relevant factors that affect the analysis.

1.2.3 Organization of the work

Chapter 2 presents useful theories for interpretation of the objectives and results contained in this work. A simplified analysis of reverse power flow is exposed in order to emphasize important observations regarding the influence of the feeders lines in the efficiency of volt-var. There is also a short description of photovoltaic systems and solar cells themselves, as well as of inverters from a power flow analysis perspective. IEEE 1547 and its requirements directly related to this work, such as volt-var and the reactive power priority mode, are also discussed. Chapter 3 presents the methodology adopted for the choice of the proposed feeders as well as the photovoltaic systems allocation and general guidelines followed during the simulations.

Finally, chapters 4 and 5 deal with, respectively, the exhibition and discussion of the results, and the synthesis of the inferences suggested by them.

The appendix A presents more detailed information about the anisotropic-model based algorithm used for transposal of solar irradiance in direction of a tilted photovoltaic panel plane.

2 THEORETICAL FUNDAMENT

2.1 Simplified reverse power flow analysis

As mentioned in chapter 1, it is known that the presence of distributed energy resources may cause overvoltage issues due to the reverse power flow induced by them. The following simplified analysis for a single-phase distribution line, represented in figure 1, discuss this phenomenon.

Figure 1 – Diagram of a single-line feeder, with terminal voltages, respective to a common neutral point, equal to $\dot{\mathbf{V}}_\mathbf{s}$ and $\dot{\mathbf{V}}_\mathbf{k}$. Without loss of generality, $\dot{\mathbf{V}}_\mathbf{s}$ can be considered as a voltage source supply. Also, a current $\dot{\mathbf{I}}$ corresponding to a flow of active P and reactive Q powers passes through the line.

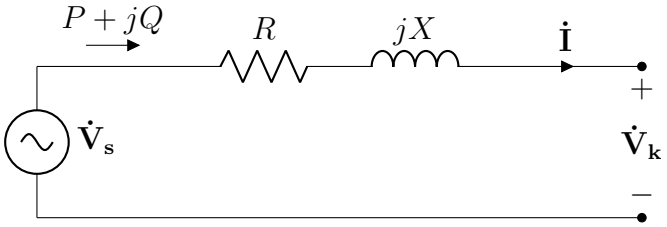

Source: the author.

In figure 1, the voltage magnitude at the end of the line is given by equation (1):

$$|\dot{\mathbf{V}}_\mathbf{k}|^2 = (\dot{\mathbf{V}}_\mathbf{s} - (R + jX) \cdot \dot{\mathbf{I}})^* \cdot (\dot{\mathbf{V}}_\mathbf{s} - (R + jX) \cdot \dot{\mathbf{I}}) \tag{1}$$

This equation can be rewritten in terms of the apparent power components P and Q, resulting in equation (2):

$$|\dot{\mathbf{V}}_\mathbf{k}|^2 = |\dot{\mathbf{V}}_\mathbf{s}|^2 - \underbrace{2(RP + XQ)}_{\dot{\mathbf{V}}_\mathbf{s}^* \cdot (R+jX)\dot{\mathbf{I}} + \dot{\mathbf{V}}_\mathbf{s} \cdot ((R+jX)\dot{\mathbf{I}})^*} + \underbrace{\left(\frac{(R^2 + X^2)(P^2 + Q^2)}{|\dot{\mathbf{V}}_\mathbf{s}|^2} \right)}_{|\boldsymbol{\Delta}\dot{\mathbf{V}}_\mathbf{sk}|^2} \tag{2}$$

where $\boldsymbol{\Delta}\dot{\mathbf{V}}_\mathbf{sk}$ is the difference between voltages $\dot{\mathbf{V}}_\mathbf{s}$ and $\dot{\mathbf{V}}_\mathbf{k}$. It is important to note that, on practical distribution feeders, voltages drops in lines have magnitudes far lower than the voltages themselves. More specifically,

$$|\boldsymbol{\Delta}\dot{\mathbf{V}}_\mathbf{sk}| << |\dot{\mathbf{V}}_\mathbf{s}| \tag{3}$$

and

$$|\boldsymbol{\Delta}\dot{\mathbf{V}}_\mathbf{sk}| << |\dot{\mathbf{V}}_\mathbf{k}| \tag{4}$$

As a consequence of equations (3) and (4), the second term from the right side of equation (2) can be neglected, resulting, after rearranging its terms, in expression (5):

$$|\dot{\mathbf{V}}_\mathbf{s}|^2 - |\dot{\mathbf{V}}_\mathbf{k}|^2 \cong 2(RP + XQ) \tag{5}$$

Initially, let the influence of Q, in equation (5), be ignored. As long as P is positive, indicating that the active power flows in direction to the load, then $|\dot{\mathbf{V}}_\mathbf{k}|^2$, relative to $|\dot{\mathbf{V}}_\mathbf{s}|$, should decrease, as expected in a traditional power flow. However, if P is negative, or, in other words, reverse power flow occurs, then $|\dot{\mathbf{V}}_\mathbf{k}|^2$ should, relative to $|\dot{\mathbf{V}}_\mathbf{s}|^2$ (which is fixed), increase proportionally to the line resistance, R. This formulation can explain the voltage rise observed in feeders when the active power flow is reversed.

Equation (5) also suggests a method to cope with this phenomenon. Considering that P is negative, if reactive power is also made to circulate through the line, in the opposite direction of active power (i.e, from the source to the load), then an undesired voltage rise can be mitigated. In fact, for the case considered in figure 1, it can be completely eliminated, by choosing Q' according to equation (6):

$$Q' = -\frac{R}{X}P \tag{6}$$

Although derived from a simple model, which does not consider coupling effects between other phases, equation (6) is of extreme importance, because it provides a method for understanding how efficient is reactive power injection for voltage regulation. Systems having components with high $\frac{X}{R}$ ratios need a very small amount of Q from its regulation assets, such as STATCOMs or static var compensators (SVCs), to support voltage regulation, something which contributes to lower their ratings. Not only that is the only benefit, but also the overall feeder efficiency is higher, because, with less reactive power circulating, lines losses are reduced, as well as cables and transformers ratings.

2.2 Modeling of cables impedances

There are several algorithms that can be used to solve a power flow (PF). In radial distribution systems, the forward-backward sweep method, which rely on modeling of the feeder lines and transformers as quadripoles, can be used. Impedance-matrix-based methods, however, also are considerably significant. It is possible, also, to use the Newton algorithm, based on the use of Jacobian matrices, to solve a PF.

Although they are significantly different, these methods share a basic set of ingredients from a feeder elements, which are their respective primitives impedance matrices, $\mathbf{Z}_p$, that define the relation between their terminals currents and respective voltages drops, according to equation (7)

$$\mathbf{\Delta V}_{abc} = \mathbf{Z}_p \mathbf{I}_{abc} \tag{7}$$

where $\mathbf{\Delta V}_{abc}$ and $\mathbf{I}_{abc}$ are, respectively, the three-phase voltage drops and currents flowing through the element.

A detailed discussion about how to model the elements within a distribution system is not intended in this section. However, a brief review of what can affect its lines primitives impedance matrices may enrich the discussion proposed by this work.

The main parameters of a single-phase line, in the frequency domain, are its resistance, inductance and capacitance. The resistance of a conductor, per unit length, can be determined from an appropriate table, or by using equation (8):

$$R_{cond} = \frac{\rho}{S} \tag{8}$$

where ρ is the resistivity of the material and S, its surface area, assumed to be constant.

The self-inductance of a conductor can also be determined in a straightforward manner:

$$L_{cond} = 2 \cdot 10^{-7} \ln\left(\frac{1}{GMR_{cond}}\right) \tag{9}$$

where GMR_{cond} is its geometric mean radius.

It is also necessary to consider coupling effects between phases. In the distribution level, transposition of lines is uncommon, resulting in the introduction of unbalance between the lines impedances, caused by a stronger magnetic coupling between a pair of phases in relation to another. The mutual inductance between phases i and j is given by equation (10):

$$L_{ij} = 2 \cdot 10^{-7} \ln\left(\frac{1}{d_{ij}}\right) \tag{10}$$

where d_{ij} is the distance between conductors i and j.

Equations (8) and (9) indicate parameters that affect the resistance and self inductance of a conductor. More importantly, increasing the cross-section surface area should cause a greater reduction of the resistance than in comparison with the inductance. Recalling that, in section 2.1, the effectiveness of reactive power to compensate the voltage rise effect during reverse power flow depends on the $\frac{X}{R}$ ratio of the elements for which power flows through, This suggests that, as long as the voltage level is fixed, feeders with higher capacity to serve loads should also be able to cope better with reverse power flow using reactive-power-based methods.

Another important remark is that the self-inductance predominance in the primitive impedance matrix, in comparison with the mutual counterparts, should increase with the voltage level of the section of the system being considered. This statement can be explained by analyzing equation (10). In order to avoid insulation rupture, because of a high voltage difference and little distance between two conductors, it is necessary to increase their spacing, and, hence, L_{ij} should decrease.

Finally, it should be noted that the actual impedance matrix of a poly-phase line segment is composed considering an appropriate superposition of all its contributions determined using equations (8), (9) and (10), as well as, possibly, the use of a Kron reduction, which embed the effects of the neutral conductor resistance and inductance in other phases, and Carson equations. However, it is still reasonable to assume that the conductors resistances and self-inductances greatly impact the diagonal elements of the matrix, specially if considering medium or high-voltage sections.

2.3 Photovoltaic systems

Solar cells are devices that, through the photovoltaic effect, convert solar irradiance into electrical energy. Photovoltaic system (PV system), on the other hand, is a term that refers to a group of solar cells, grouped in panels, together with an electronic subsystem that manages extraction and destination of energy from them. Although not mandatory, they may also include a battery energy storage system, an usual addition in off-grid applications [15]. Figure 2 presents a generic division of a PV system sub components.

Figure 2 – Generic photovoltaic system sub components diagram. The arrows indicate possible directions for power flow. Note that the red arrow is bidirectional only if a battery energy storage is present.

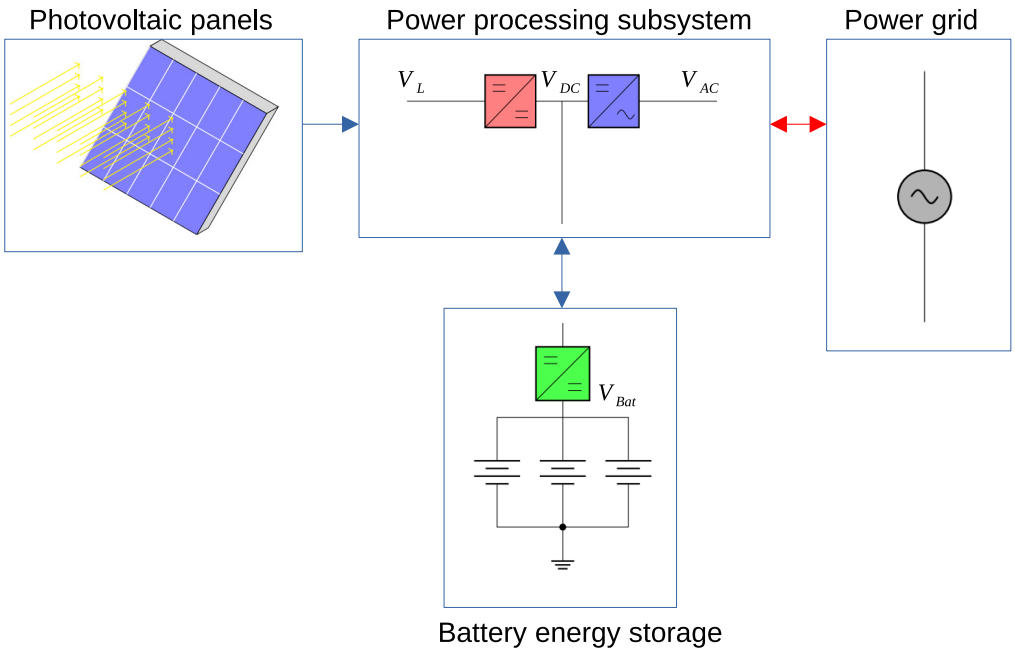

Source: The author.

The power output from those devices depends on several factors. The most important is the incident irradiation, for which linear relationships are assumed from a practical point of view [16]. Temperature also exerts a considerable influence (if observed over a wide range). Finally, the equivalent load seen by the cell is also very relevant. The last affirmation can be better understood by analyzing its behavior when it is supplying

energy. For this intent, there are different models, each one with varying degrees of complexity, although the simple single-diode model, depicted in figure 3, is sufficient. In the figure, the connected load, R_L, is also included.

Figure 3 – Single-diode model of a solar cell. I_P is the photo generated current, I_D, the dark current, R_{sh} and R_s are resistances considered due to imperfections in the cell junction and casing, respectively, and R_L is the connected load.

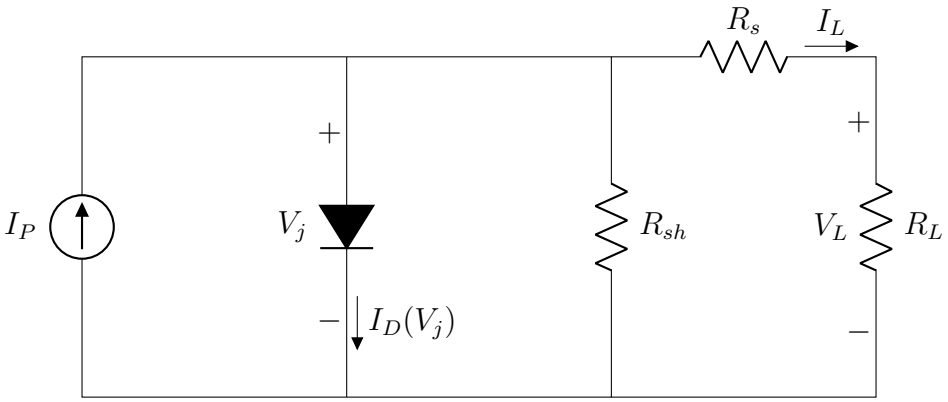

Source: The author.

The cell output voltage, considering the model represented by figure 3, is related to its output current according to equation (11):

$$-V_L + R_{sh} \cdot \left[I_P - I_D + I_L \left(1 + \frac{R_s}{R_{sh}} \right) \right] = 0 \tag{11}$$

In this equation, I_P is assumed to be proportional to the cell input irradiation, and I_D is the device dark current, given by equation (12):

$$I_D = I_0(e^{k \cdot V_j} - 1) \tag{12}$$

where I_0 and k are appropriate parameters for a given physical realization of solar cell, and V_j is its junction voltage. Figure 4 shows an example of I-V curve, as well as its corresponding $I - P$ characteristic, considering equation (11) as reference.

Figure 4 – Typical solar cell $I - V$ and its corresponding $I - P$ curves for a given I_P. The latter is labeled as the "knee-curve", in allusion to its format.

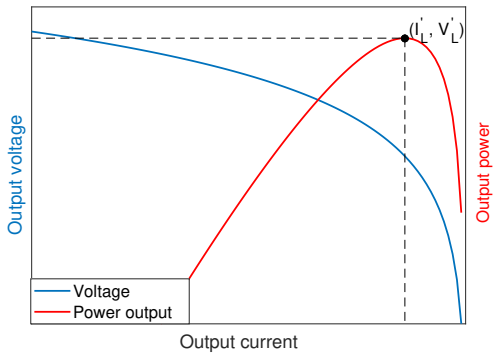

Source: The author.

Equation (11) and figure 4 are important, because they show that a solar cell power output depends not only on its characteristics, but also on the load R_L. For each one of these curves, there is a pair (I'_L, V'_L) with maximum product. The mentioned pair is defined as the maximum power point, and the value $V'_L\ I'_L$ is the power of maximum power point (P_{mpp}).

It is of interest, in order to optimize extraction of energy from a PV system, to always operate following the maximum power point. Tracking of it can be achieved by dynamically controlling the load that is seen by the array (in other words, changing the electrical equivalent of R_L in figure 3), a capacity possible for power electronic devices, such as a boost converter.

It is required a minimum time for the electronic components of a PV system to track its panels maximum power point in a given situation. However, this period can be considered as far inferior to power flows typicals timesteps. Hence, it will be assumed, for the rest of this work, that P_{mpp} can be achieved instantly. The previous statement also implies that, as long as the referred incident irradiation level and module temperature are concisely specified, this variable can be safely considered as a definition of a PV panel power rating (in fact, this is how commercial panels ratings are informed).

2.4 Transformers and tap changers

Transmission systems should aim to deliver electrical energy while minimizing losses from the transmission process. The apparent power provided by a substation is simply the product of its phases currents and voltages phasors:

$$S = \sum_{k=0}^{n} \dot{\mathbf{V}}_\mathbf{k} \cdot \dot{\mathbf{I}}^*_\mathbf{k} \tag{13}$$

where $\dot{\mathbf{V}}_\mathbf{k}$ and $\dot{\mathbf{I}}_\mathbf{k}$ are the phases voltages and currents, respectively. Losses dissipated as heat by conductors, however, increase proportionally with the magnitudes of the currents. This makes desirable to maintain a high-voltage level for as far as possible through the electrical power system, which, in the other hand, conflict with safety requirements in the proximities of the consumption regions. The standard solution for this dilemma is to employ a transformer.

The transformer is a device capable of efficient conversion of AC voltage magnitude level. The presence of this device in a distribution system is so ingrained that it is not easy to plan a power grid having the same efficiency without it. Power flow programs may use generalized methods for determination of the impedance matrix for an arbitrary number of windings that do not require having an equivalent circuit as an intermediate element, but, as much as ingrained as it is the transformer, the same could be said to its

equivalent circuit, for two-winding and three-winding types, depicted, for the single-phase two-winding model, in figure 5.

Figure 5 – Two-winding transformer equivalent circuit.

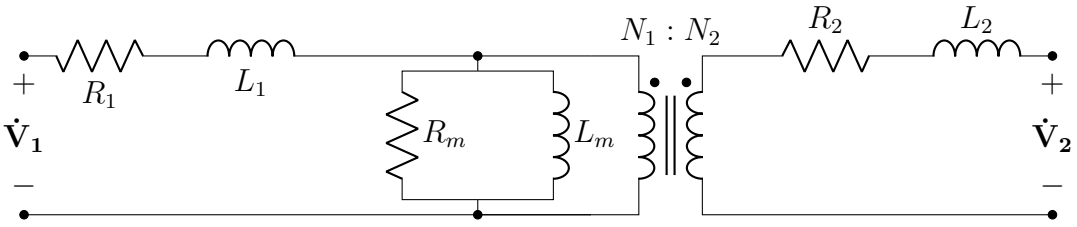

Source: The author.

For the ideal transformer, obtained by assuming that the values of R_1, X_1, R_2, X_2, R_m and X_m are zero, the voltage magnitudes between its primary and secondary windings are related through equation (14):

$$\frac{|\dot{\mathbf{V}}_\mathbf{1}|}{|\dot{\mathbf{V}}_\mathbf{2}|} = \frac{N_1}{N_2} \tag{14}$$

Equation (14) and the model represented by figure 5 are widely known. What is intended to discuss in this section, however, is how, through the dynamical manipulation of N_2, a transformer can be used as a voltage regulation device.

Tap changers are components used to adjust the number of windings N_2 in order to maintain the voltage output of the transformer, V_2, within a desired range. There are three-phase as well as single-phase tap changers. Usually, three-phase models, which are more common, measure variables of only one of the phases (for example, phase A) and use these measurements as inputs to its regulator, although there is a tendency in employing separate, per-phase regulators [17]. The way which the measurements are used, however, can be different, as will be explained in the next paragraph.

Without considering interactions with other EPS assets, in traditional grids, the voltage profile, while traveling through a feeder line, has a monotonic behavior, i.e, voltages consistently drop from its start until the furthest consumer located at the end. Hence, it is desired, in this case, to regulate not the voltages measured at the secondary terminals of the transformer whose taps are being controlled, but the ones being served in the end. Line drop compensators are elements present within tap changers that account for the voltage between the measured terminals and the point of interest, through the measurement of, alongside of the transformer voltages, its corresponding currents. The modified voltage to be controlled by the tap changer regulator is calculated according to equation (15):

$$\dot{\mathbf{V}}_\mathbf{reg} = \dot{\mathbf{V}}_\mathbf{in} - (R_{LDC} + jX_{LDC}) \cdot \dot{\mathbf{I}}_\mathbf{in} \tag{15}$$

where R_{LDC} and X_{LDC} are parameters related to the impedance between the transformer and the point of interest, as well as the bandwidth B_W, the regulation set-point V_{ref}

and the reliability required by the application. The parameter B_W is an error deadband threshold between $|\dot{\mathbf{V}}_{\mathbf{reg}}|$ and V_{ref}, under which the tap changer should not take action, in order to avoid unnecessary operations.

Tap changers have proven to be extremely effective in improving voltage regulation of traditional grids. However, the operation of a LDC may impact the demand that is required of a DER contributing to voltage support through the use of reactive power. For example, improper matching between tap changers and volt-var setpoints may result in a demand higher than the necessary from both types of elements, which would negatively impact how much energy the DERs may produce. Or, in the other hand, since they are capable of improving the regulation of the subsequents sections of a feeder, it is reasonable to think that using them in a proper way could also reduce the necessity of active power curtailment from DERs. Nevertheless, it is valid to try to evaluate how they may influence the distributed generation, and, more importantly, how should they impact different sections of a feeder.

2.5 Capacitor banks

Considering equation (5) from section 2.1, it is expected that a voltage drop due to the flow of active power can be mitigated by the injection of reactive power to the grid ($P > 0$ and $X < 0$). Usually, consumers are restricted of this possibility since they are required to maintain a high power factor. However, the distribution system operator may employ devices such as capacitor banks and other similar classes of static compensators in order to improve the voltage regulation within its feeder.

Capacitors are capable of providing fixed amounts of reactive power to the grid. Usually, they operate considering an hysteresis-based control algorithm in which the capacitor bank is switched on if the voltage measured at its PCC is lower than a threshold. Then, the asset remains connected to the grid until the measured voltage surpasses a second threshold. A deadtime is normally considered in order to avoid unnecessary switchings due to transients.

If a DER, complying with a voltage support algorithm, is connected to the same bus as a capacitor bank, it can be relieved from its requirement by the action of the bank when there is an undervoltage. However, a different outcome should happen if there is an overvoltage. Since only the difference between the DER and the capacitor bank reactive power outputs affects the grid voltages, the latter should need to absorb more reactive power in order to achieve a desired effect if the former remains interacting with the power system. What is to be evaluated, hence, is how strongly would be the impact in the curtailment of energy generation for such cases.

Figure 6 – Fluxgram of a typical switched capacitor bank operation algorithm

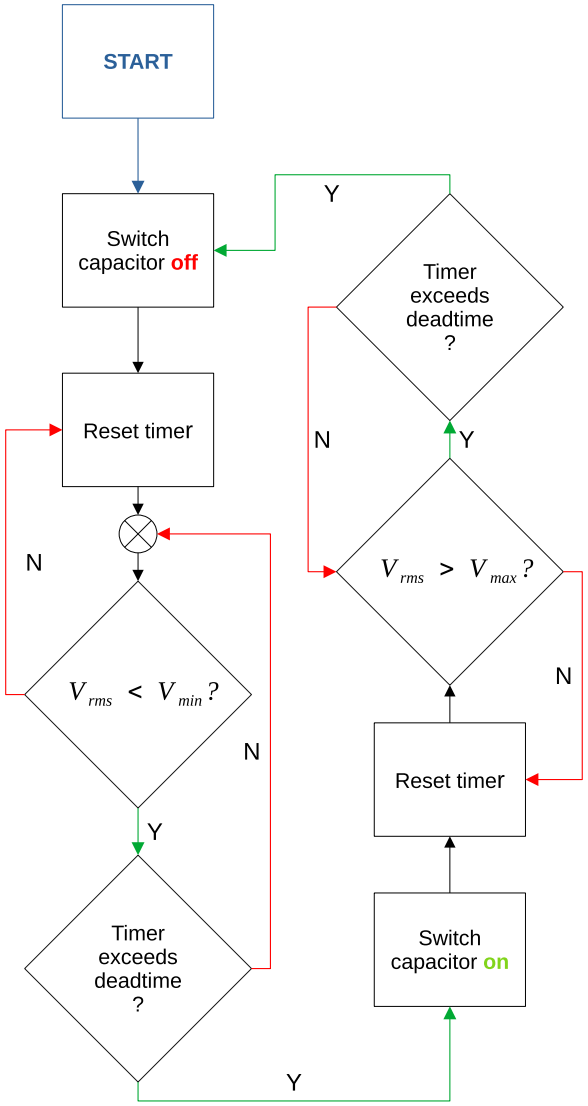

Source: The author.

2.6 Determination of the irradiation available to a PV panel

The density of solar irradiation that arrives at Earth, before entering the planet atmosphere, can be considered, for practical purposes, as almost constant, even during different seasons [16]. However, until it reaches the planet surface, part of it is absorbed, while another is refracted, changing its direction. The result is that there are different components that reach a photovoltaic cell sensible surface. Consequentially, they must be superposed according to their contributions, as specified by equation (16):

$$Irrad(t) = Irrad_{DNI}(t) + Irrad_{DHI}(t) + Irrad_{\text{Albedo}}(t) \tag{16}$$

In equation (16), $Irrad_{DNI}$ is related to the direct normal irradiance (DNI), which is the portion of the sun rays that retains its original direction. $Irrad_{DHI}$, on the other hand, is determined based on the diffuse horizontal irradiance (DHI), the scattered portion. $Irrad_{\text{Albedo}}$, at last, corresponds to the share that reaches the ground and is reflected back in direction to the panel sensitive area. Figure 7 illustrates these components.

Figure 7 – Graphical representation of the solar irradiation components DNI, DHI and Albedo. Note that not necessarily any of those components incide orthogonally to the PV panel represented in the figure.

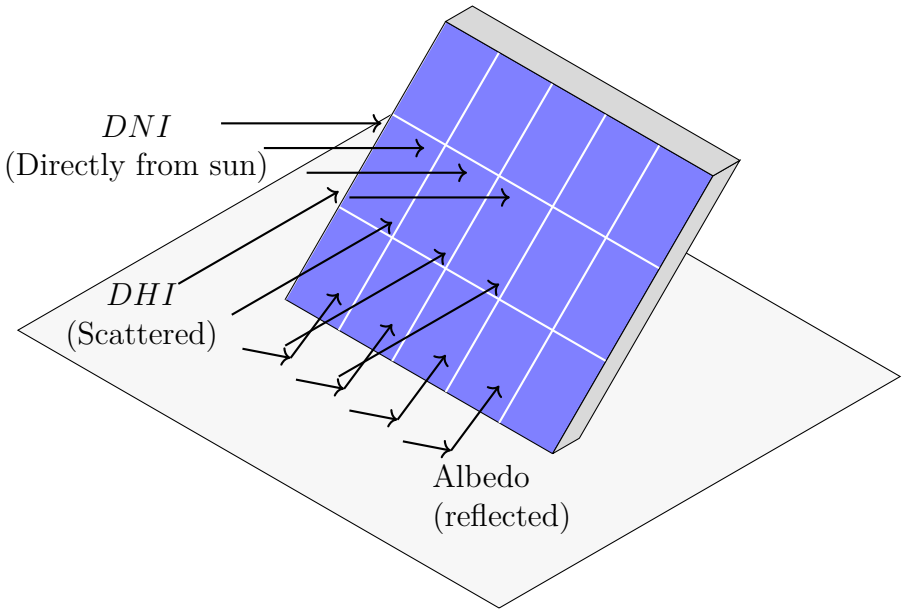

Source: The author.

The contribution of DNI to a PV panel irradiance input is the value of its projection oriented towards the panel plane:

$$Irrad_{DNI} = DNI \cdot cos(\theta_S) \tag{17}$$

where θ_S is the angle of incidence between the sun beam and the panel, which can be calculated using equation (18):

$$\cos(\theta_S) = \cos(\gamma_S)\sin(\gamma_{PV}) + \cos(\gamma_{PV})\sin(\gamma_S)\cos(\alpha_S - \alpha_{PV}) \tag{18}$$

In equation (18), the variables γ_S and γ_{PV} represent the zenith angles of the sun and the photovoltaic panel, relatives to the location surface, while α_S and α_{PV}, the azimuth angles of the same bodies. It is useful to emphasize that these variables are normally specified according to an inertial bystander located at earth. Hence, for fixed mount panels, γ_{PV} and α_{PV} are fixed, while γ_S and γ_{PV} change with time.

Equation (17) implies that, in order to calculate $Irrad_{DNI}$, it is necessary to know the angular solar position through time. There are available, in the literature, astronomical publications containing data that can be used for its determination. However, algorithms for prediction of the required variables can also be implemented, with negligible discrepance

in comparison with measurements. In particular, the algorithm explained in [18] was adopted in this work.

There is, in the literature, a general consensus about how to transpose the DNI contribution to a panel plane [19]. However, the same cannot be affirmed for the case of DHI. Normally, it is assumed that the distribution of DHI, in the sky, is isotropic, or, in other words, that the direction considered is not relevant. As a corollary, the DHI-provenient transposed irradiance of a PV panel can be calculated using equation (19):

$$Irrad_{DHI} = DHI \cdot \left(\frac{1 + \cos\left(\gamma_{PV}\right)}{2} \right) \tag{19}$$

where γ_{PV}, as mentioned for equation (18), is the panel tilt angle.

It is important to comment that, even though equation (19) is most widely used, it was identified that the value of $Irrad_{DHI}$ calculated using this formula consistently underestimates the real contribution of this component, due to the assumption of sky isotropy. Because of this, several more complex extensions, also known as anisotropics models, were proposed, such as the model developed by [20], which was shown to be more consonant with experimental data [21], and, hence, it was adopted in this work as the procedure used for DHI transposal to a tilted plane. More information about this algorithm can be found in the appendix A.

The share of irradiance originated from the albedo component, finally, can be determined using equation (20):

$$Irrad_{\text{Albedo}} = \rho \left(\frac{1 - \cos(\gamma_{PV})}{2} \right) \tag{20}$$

where ρ is the albedo factor, which is influenced by the surroundings of the panel of interest. Although the use of a constant value is effective in calculations of monthly or yearly averages, this methodology is not considered adequate for small intervals. Also, due to the inherent difficulty in determining an appropriate albedo factor, this component will be ignored.

2.7 Inverters

Even though the contribution of elements aiming to maximize power extraction is relevant, for AC grid-tied PV systems, the most important of its electronic components is the inverter. With it, a photovoltaic system can interact with the electrical power system which it is connected to.

Inverters are related to innumerous types of applications involving power grids in some way. For example, they are key components in most time-domain power quality correction systems [22]. Information about detailed modeling of this element can be found in [23, 24]. For power flows studies, or, in other words, steady-state operation, which is the

focus of this work, those devices can be considered as constant-power (PQ) current sources, capable of producing or absorbing both active as well as reactive power. Through different power flows, or even during the execution of a single one, according to the algorithm being executed by the inverter, these power components may vary. Also, it is important to note that the previous consideration implies that the units considered are of current-following type, in opposition to grid-forming.

The flexibility of inverters in injection and absorption of active and reactive power, as well as their fast dynamic response, are reasonable reasons to justify their attractiveness for voltage conditioning applications. In particular, there are several studies regarding their use solely for reactive-power-based voltage compensation (as a D-STATCOM) and even, in conjunction with a battery energy storage system (BESS), as an active and reactive power compensator for grid support.

There is, inherently in a physical power converter, a maximum rating of power processing that cannot be surpassed without causing damage to it. For inverters, this limit is normally specified in kilo Volt-Ampere (kVA) units. The inverter apparent power output, in the context of power flow analysis, is defined by equation (21):

$$S = \sqrt{P^2 + Q^2} \tag{21}$$

where P and Q correspond to, respectively, the active and reactive powers being processed by it. Equation 21 defines a circumference of radius S centered at the origin. The circumference, as well as its inner area, compose the inverter capability region.

2.8 IEEE 1547-2018™ standard

With the growth of consumers owning distributed energy resources, specially PV systems, concerns regarding reversion of active power flow (from the consumers location) have arose between EPS operators.

IEEE 1547-2018™ is a standard concerned with the specification of a minimum set of capabilities inverters should have when used for connecting DERs with the grid, so that they are able to provide support to the grid during transients and steady-state operation. Figure 8 show the hierarchy of the requirements proposed by the document.

The higher precedence is given to tripping capabilities, related to conditions for which the inverter have to, within a maximum tolerance time, stop interacting with the EPS. Ride-through requirements are concerned with time-domain-related parameters, such as instantaneous frequency change. Voltage-active power requirements involve the direct curtailment of active power, without regard of using reactive power instead, if requested by the EPS operator. The last position is occupied by the class of algorithms that use reactive power for voltage support. Among them is volt-var.

Figure 8 – Hierarchy of requirements as specified in 1547-2018™ standard

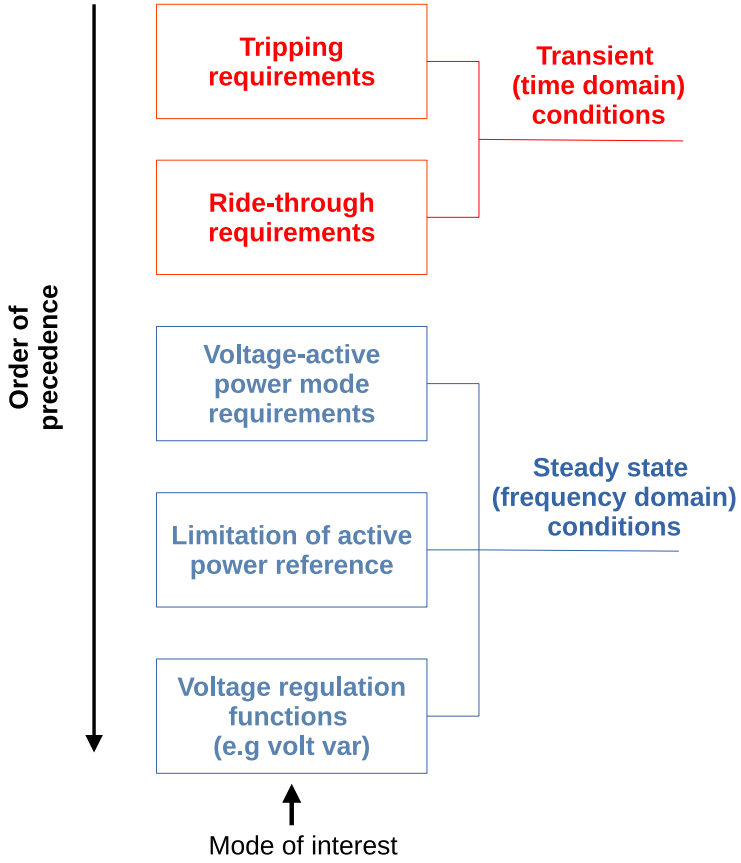

Source: The author.

2.8.1 Volt-Var control mode

The volt-var algorithm can be interpreted as a configurable piece-wise linear controller. The reactive power reference is a function of the calculated average of the PCC effectives voltage magnitudes [8]. In mathematical terms,

$$Q = f(\bar{V}) \tag{22}$$

and

$$\bar{V} = \frac{1}{N}\sum_{k=1}^{N} V_k \tag{23}$$

where N represent the number of phases of the inverter, and V_k is the k-th RMS phase voltage magnitude.

IEEE 1547 standard suggests the division of DER units, for voltage regulation functions, in two categories. Category A concerns DERs in a low penetration scenario, with reduced requirements, while category B, recommended for higher DER penetration

cases, is more exigent. Figure 9 shows two shapes of voltage-to-reactive-power curves. Each one pertains to one of the two mentioned groups.

Figure 9 – Voltage-to-reactive-power functions for category A and B DERs.

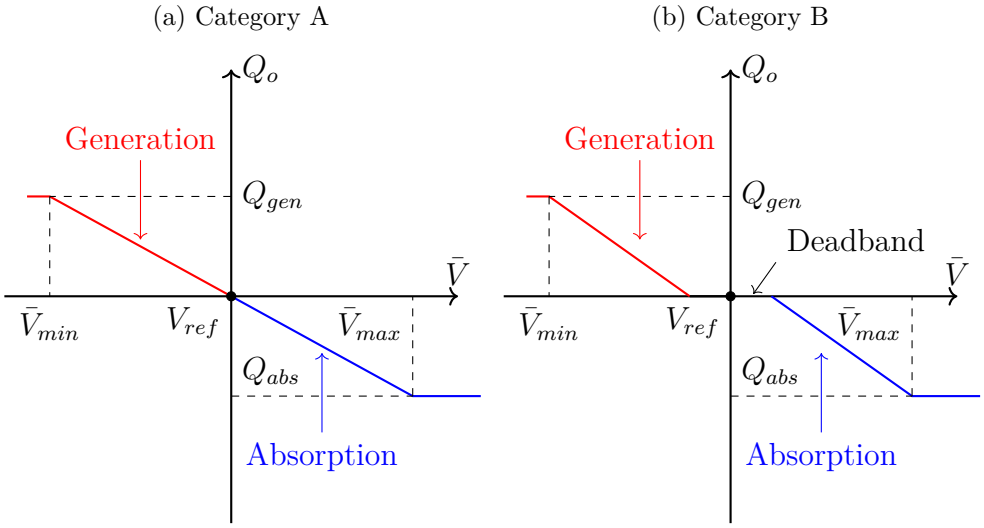

Source: The author.

The main differences between the two curves exhibited in figure 9 are the presence of a deadband (for category B) and the recommended default maximum VAR absorption (Q_{abs}), although it is also demanded the ability to configure these values based on specifications provided by the EPS operator responsible for the region where the considered unit is operating

According to a PV panel available irradiation, its corresponding inverter will be capable to supply a certain value of active power to the grid. However, it may also be required, depending on the local conditions of the voltages at the PCC, the injection of a quantity of reactive power by the unit which would result in a violation of the inverter capability curve if it continues to maintain the same active power level. As required by the standard, it is necessary, then, to curtain the injection of a portion of the available active power in order to prioritize the reactive power. The resulting difference in energy that could be produced, during this time, considering that there is not any energy storage system involved, will be lost. Figure 10 illustrate how the inverter operating point is displaced under the previous considerations.

The standard requires that, by default, only until a certain point the DER unit inverter must curtain its active power injection in order to comply with the reactive power output requirement. This region of mandatory compliance, for category B of DERs is exhibited in figure 11. Note that although the figure refers to category B, the only difference in comparison with category A is the mandatory reactive power absorption limit, which is lower (25% of the nameplate capability of the inverter, instead of 44%). Also, it is important to note that, although not explicitly required by the standard, the curtailment limits, as delimited in figure 11, can be adjusted.

Figure 10 – Example of reduction of active power injection, due to the volt-Var reactive power prioritization requirement.

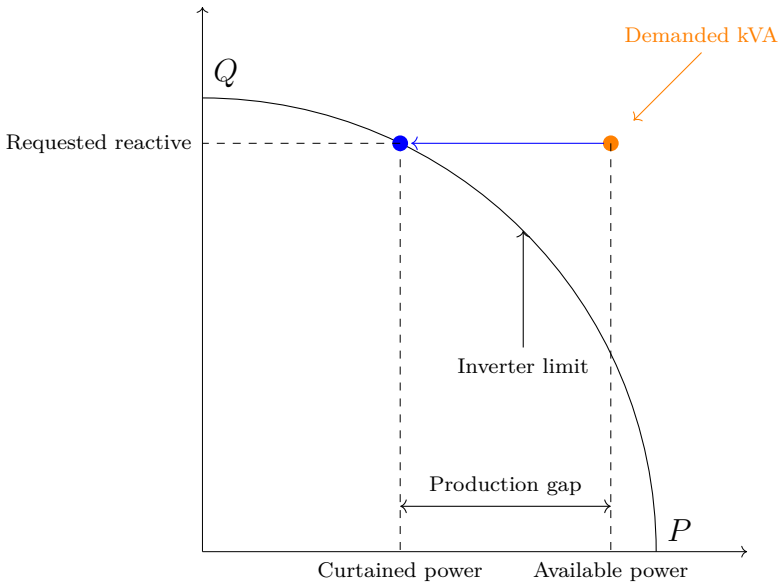

Source: The author.

Figure 11 – Mandatory reactive power priority region for category B DERs, as defined by 1547 standard.

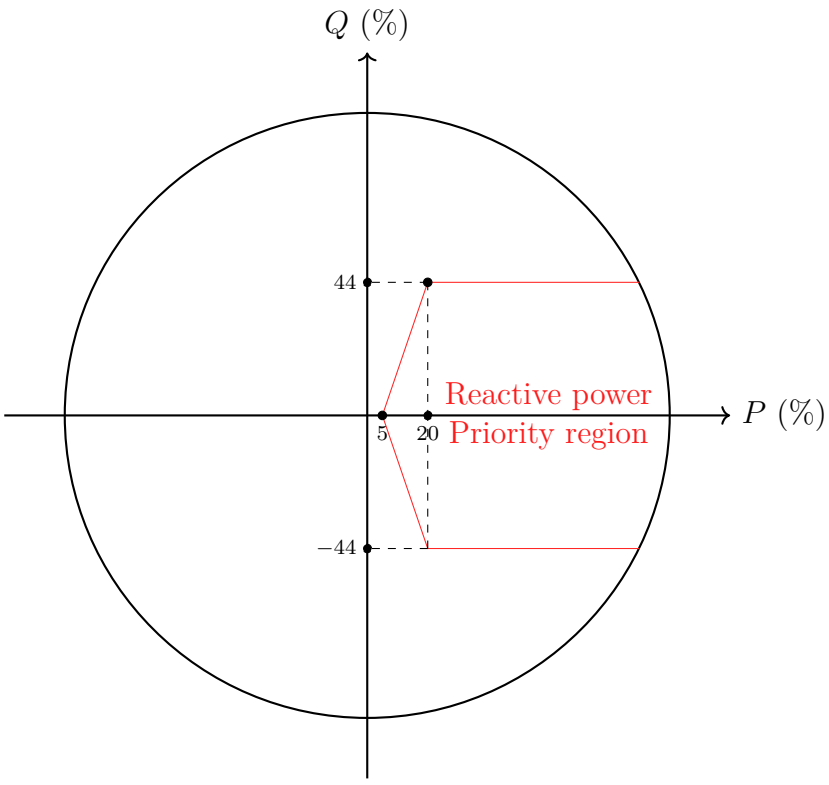

Source: The author.

It was commented in chapter 1 that there is a lack of sufficient information about the energy generation decrease due to active power curtailment, caused by conditions such as the one illustrated by figure 10. Therefore, a methodology to tackle this problem will be presented in the next chapter.

3 WORK METHODOLOGY

It can be expected, according to the discussion in chapter 2, that the use of volt-var during peak generation periods should result in active power curtailment of inverter-based distributed energy resources units, such as PVs. Also, a few factors that could affect this outcome were exposed, such as the $\frac{X}{R}$ ratio of the feeders conductors impedances, seasonal variations of solar irradiation available to the PVs, as well as the influence of assets owned by the EPS operator, such as tap changers and capacitor banks. Hence, as an attempt to improve the quality of the analysis proposed in this work, three different feeders were populated with photovoltaic systems and simulated in a full-year scenario. Section 3.1 presents an overview of the proposed feeders, as well as a short description of their characteristics. Section 3.2, on the other hand, focuses in the specification of the conditions considered during the execution of the simulations.

3.1 Feeders descriptions

The following subsections present the test cases considered for use in this work, along with the reasons considered to justify their inclusions.

3.1.1 IEEE 13 Bus test case

The IEEE 13 Bus test case is a small model. Although its lines are short, it is highly loaded, and hence it still presents voltage regulation issues. It operates, mainly, at the 4.16kV level, although one of its buses is connected through a step-down transformer. Figure 12 shows a diagram of the feeder.

Figure 12 – Diagram of the IEEE 13 Bus test case

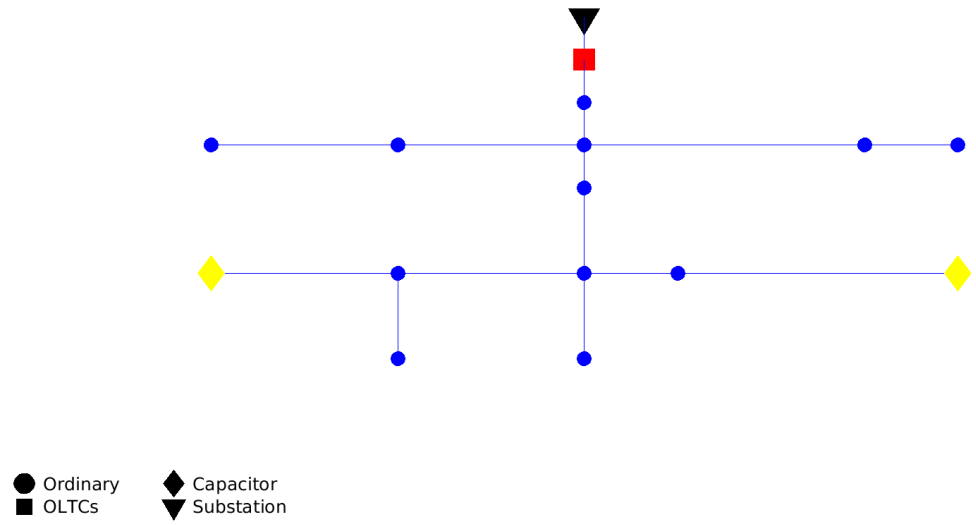

Source: The author.

The figure 13 exhibits an histogram of the phase-neutral voltages of the system under nominal load conditions. It can be observed that there is a high variance of the

magnitudes in the histogram, with a considerable presence of overvoltages (caused by the tap changers operation) and undervoltages, which can be considered as an evidence of the high loading of the feeder.

Figure 13 – Histogram of IEEE 13 Bus test case phase-neutral voltages under nominal load conditions.

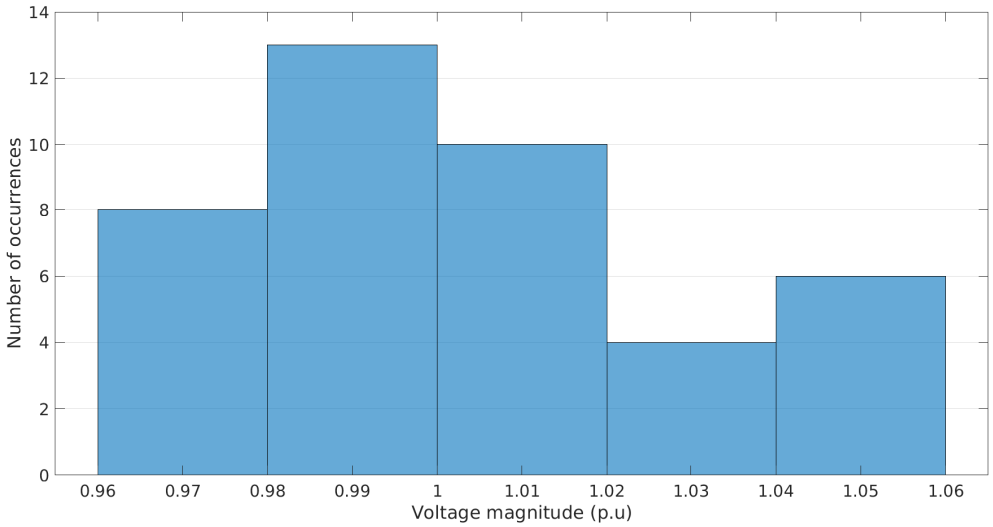

Source: The author.

Table 1 contains an indication of the loads demanded power in each phase of the feeder.

Table 1 – Power demand for each phase of the IEEE 13-Bus test case.

Phase	kW	kVAr
A	1260	691.5
B	924	599
C	1282	811.5

Source: The author.

The reason behind the inclusion of this feeder is that, although it is a robust feeder, with a very good efficacy to reactive power compensation methods, it is also highly loaded. Hence, it is expected for the impact of the feeder own voltage regulation conditions (without any DER inserted) to be more easily distinguished.

3.1.2 IEEE 34 Bus test case

The IEEE 34 Bus test case, originally based on an actual grid located on Arizona, United States of America [25], is a test feeder with long lines, as well as lightly loaded. It presents voltage regulation issues, requiring placement of regulators and capacitor banks in order to mitigate violations of reliability standards. This feeder can be considered as characteristic of rural regions. Figure 14 shows the feeder configuration, with indication of existing voltage regulation assets.

Figure 14 – Diagram of the IEEE 34 Bus test case.

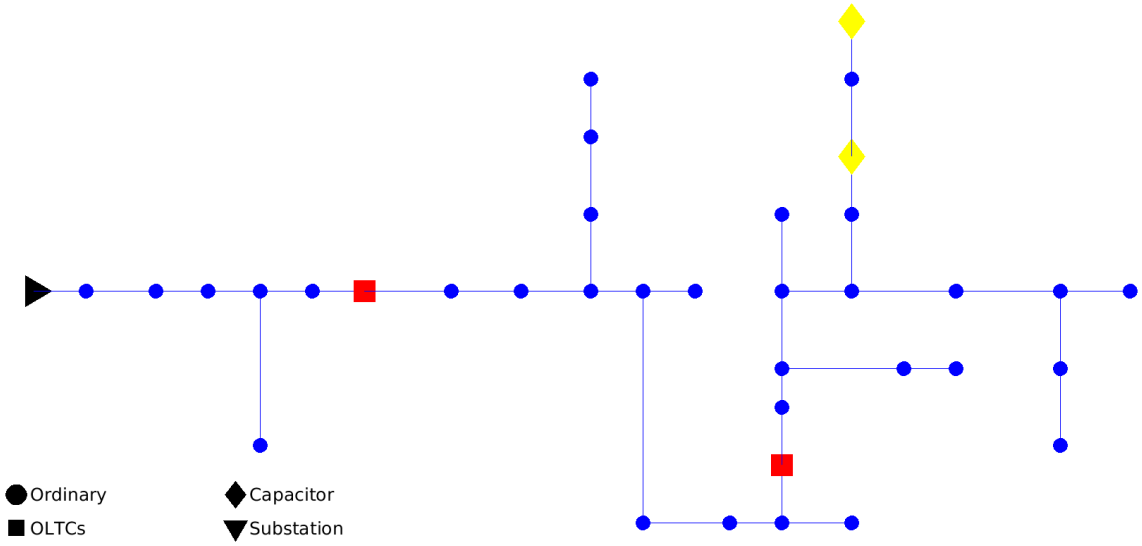

Source: The author.

The reason for this choice is not only the low short-circuit ratio of this feeder, resulting from the high length of its lines, but also because it is a weak feeder with a disadvantageous overall $\frac{X}{R}$ ratio. As mentioned previously, it has considerable difficulties in voltage regulation without any PV system inserted. Figure 15 shows an histogram of the feeder voltages, for a power flow under nominal load conditions, while table 2 indicates how the feeder loads are distributed within the phases of the system. It can be easily seen that the variance, as well as the deviations from 1 p.u of the undervoltages extremes of the histogram are higher than in comparison with both the 13 Bus feeder, which was exhibited previously, as well as the 123 Bus test case, which will be presented next.

Figure 15 – Histogram of 34 Bus test case feeder voltages under nominal load conditions

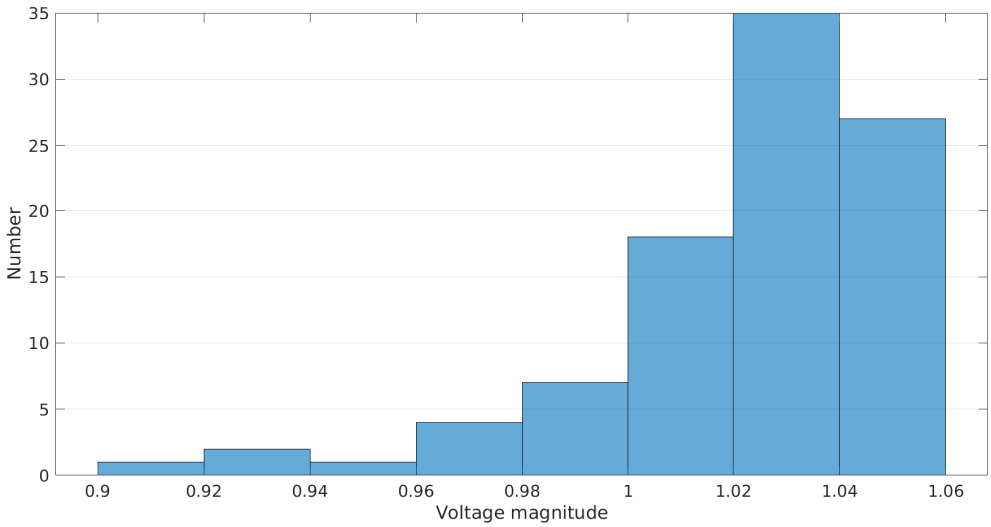

Source: The author.

Table 2 – Power demand for each phase of the IEEE 34-Bus test case.

Phase	kW	kVAr
A	328	165.5
B	250.5	124.5
C	188.5	97

Source: The author.

3.1.3 IEEE 123 Bus test case

IEEE 123 Bus test case, finally, is characterized as a medium-sized system, with notable presence of both underground and overhead lines, as well as an adequate voltage reliability. From a power flow point of view, it is considered as having a good convergence behavior. Figure 16 shows the topology of this feeder.

Figure 16 – 123 Bus test case overview.

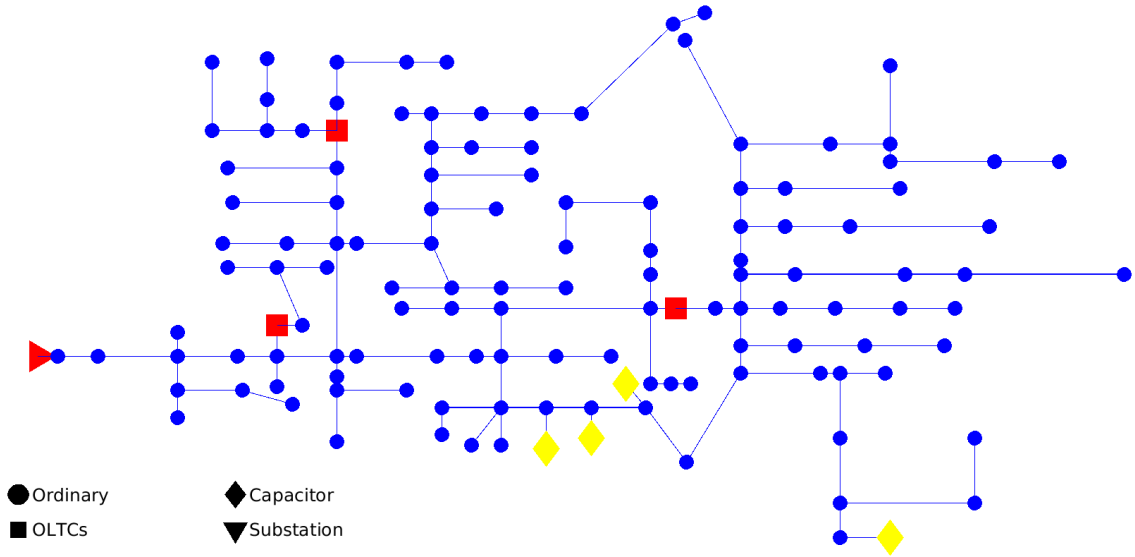

Source: The author.

Table 3 exhibits the allocation of the feeders loads, per phase.

Table 3 – Power demand for each phase of the 123-Bus test case.

Phase	kW	kVAr
A	1295	687.5
B	847.5	465
C	1032.5	542.5

Source: The author.

The feeder lines usually have higher $\frac{X}{R}$ ratios, if compared with the previous test cases. Also, although it has a total load demand similar to the 13 Bus test case, the differences between the former lines and the later ones are sufficient to consider this feeder as considerably less loaded. Choosing to study this feeder, then, should assist in the

determination of the implications of the last statements. Figure 17 depicts its voltages under nominal load conditions.

Figure 17 – Histogram of 123 Bus voltages under nominal load conditions.

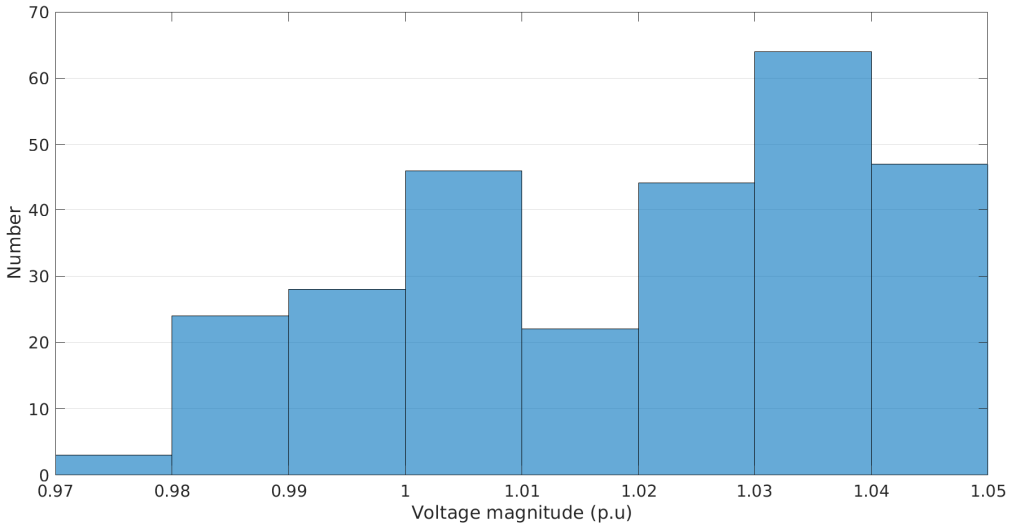

Source: The author.

Finally, table 4 can be useful to compare each feeder individuals characteristics.

Table 4 – Characteristics of each EPS considered for this work.

System	13Bus	34Bus	123Bus
Strength	Strong	Weak	Strong
Average $\frac{X}{R}$	High	Low	High
Voltage regulation	Weak	Weak	Good

Source: The author.

3.2 Simulations overview

It is proposed the execution of several different scenarios, for all three feeders. A more detailed simulation should span over a broad time range, due not only to the fact that both irradiation timeseries and loads demand curves have a significant variance over different hours of the day, but also over seasons. The contribution of this study could also be improved by analyzing the impact of irradiance distributions pertaining to different geographical regions, as well as further modeling the photovoltaic system energy processing chain, by, for example, accounting for the panels reflectance or inverter losses. However, it is sufficient, in order to fulfill the objectives delimited in chapter 1, to ignore these details.

Hence, regarding the desired objectives presented in chapter 1, an yearly simulation was considered. Also, the tasks of assigning loadshapes and irradiance curves

for the corresponding elements in each feeder were simplified by adopting the following assumptions:

1. All loads in the feeders share the same load curve;
2. The irradiance available to each PV unit is the same.

The first affirmation simplifies, due to the lack of more details about the loads connected to each EPS, the attribution of load curves. The second implies that not only all PVs solar panels would be allocated with the same orientation regarding to the sun, but also that shading and soiling effects, as well as locational differences in irradiance are ignored.

The load curve used is available within the distribution of the open-source software OpenDSS, which was also used to execute the simulations. This power flow execution program has notorious popularity in academics, due to, as mentioned, its open-source nature, as well as containing in-built models for PV systems with capabilities to not only operate according to IEEE 1547-2018 standard, but also allowing implementation of custom algorithms in quasi-static, time-series (QSTS) simulations.

The irradiation curves were taken from the National Solar Radiation Database [26], maintained by the National Renewable Energy Laboratory of the United States. The dataset, publicly available, pertains to a North America region. This location was aimed specifically due to the fact that the studied feeders, in section 3.1, were based on counterparts existing near from the dataset claimed localization. In addition, it contains a high granularity (10 minutes between measurements), an important factor for this study. Also, its location has all four seasons of the year.

The dataset contains measurements for, among other fields, DNI and DHI, as well as its geographical coordinates and measurements times. As mentioned previously, the solar energy that is made available to a PV system is a function of not only these parameters, but also of how it is positioned. A common practice for fixed arrays, in projects, is to place them in a way that maximizes the medium irradiance input over time, considering the physical restrictions which their accommodations are subjected to. As a rule of thumb, panels should be orientated facing the equator line and sloped with an angle equal to its locations latitudes. Normally, for a fixed year, the real optimum tends to agree well with this rule. Figures 18 and 19 depict, respectively, the accumulated energy, calculated using the dataset, as a function of orientation, and the same curve scaled relative to its global maximum. As mentioned previously, the difference between the practical rule and the numerically determined solution is not high.

Figure 18 – Calculated energy for different panel orientations from the irradiation dataset.

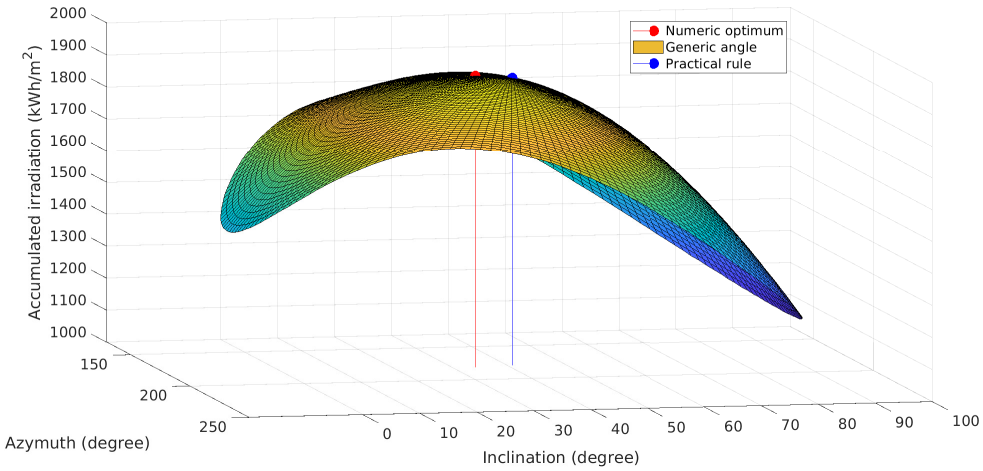

Source: The author.

Figure 19 – Calculated energy, relative to the inclination of maximum energy, from the irradiation dataset.

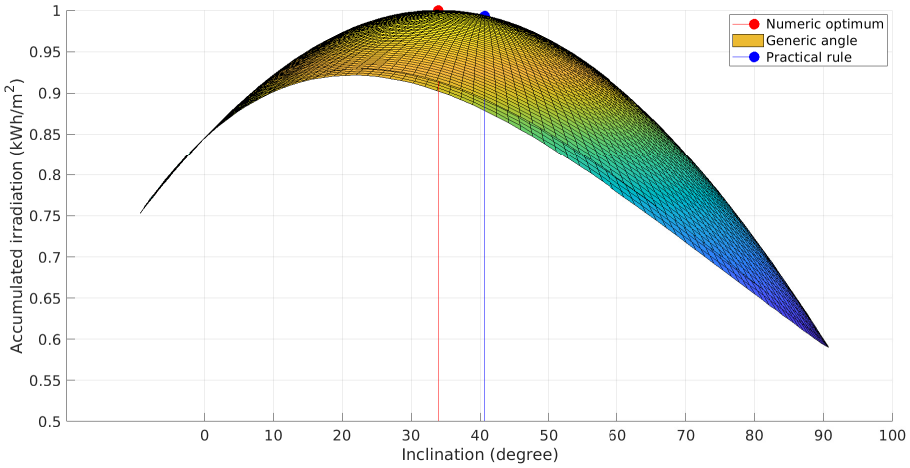

Source: The author.

The tilting angle was chosen as the slope resulted from the optimal solution with an azimuth of 180 degrees. Consequentially, the transposed irradiance timeseries employed was determined according to these pair of angles. It is useful to note, however, that this choice may slightly, although not relevantly enough, affect the distribution over the year of irradiance. More details related to this statement can be found in the appendix A.

The figure 20 shows a plot of the load and irradiance timeseries together. It can be noted that there is a higher variance of the solar irradiation than in comparison with the load timeseries. Also, the peak consumption of the loads occur close to the beginning and end of the year, which is expected from locations that present all four seasons on the northern hemisphere. Since it is winter during these periods, the increased demand from the loads can be explained by the more severe weather of this interval.

Figure 20 – Time-series of load and solar irradiation profiles.

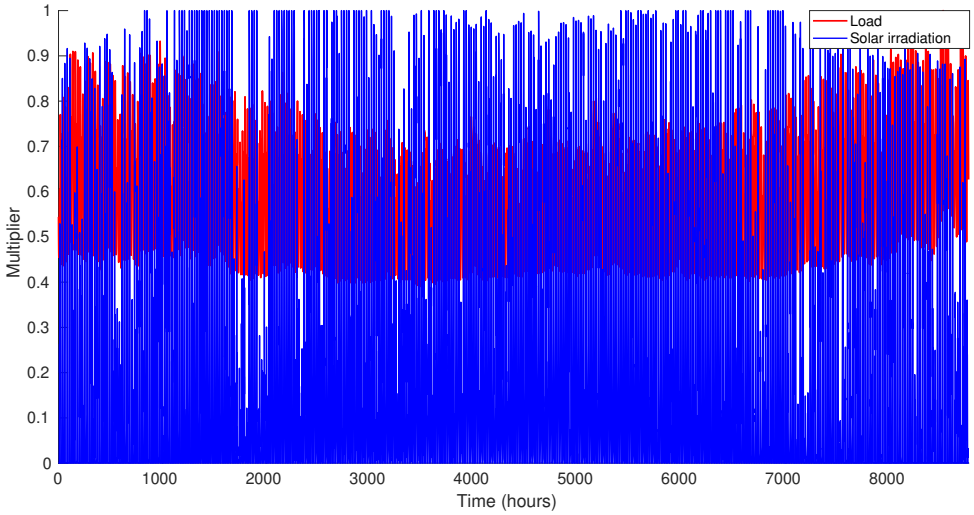

Source: The author.

A reasonable question would be if different results would be obtained for different levels of PV systems penetration. In order to answer this question, the yearly simulation as specified until now was repeated with varying PVs capacities, according to each bus total energy consumption. More specifically, for a given scaling percentage S_P, the j-th bus installed photovoltaic peak generation capacity (or P_{mpp} under maximum irradiance, equivalently), was calculated by using equation (24):

$$P_{mpp}^{j} = \left(\frac{\sum\limits_{i \in B_j} \int_0^T P_i \cdot P_{mult}(t) dt}{\int_0^T Irrad(t) dt} \right) \cdot \frac{S_P}{100} \tag{24}$$

where B_j is the set of the loads that belong to the same bus, and P_{mult} and $Irrad$ are the considered load and solar irradiation timeseries functions, as discussed previously. The time interval T in the integrals is equal to one year. For each PV system, its inverter kVA rating (S_{max}) was chosen to be equal to P_{mpp}:

$$S_{max}^{j} = P_{mpp}^{j} \tag{25}$$

It is important to note that not necessary the criteria corresponding to equation (25) may be realistic. There is only a small fraction of time, when solar irradiation is high, in which a PV panel will output a power closer to its P_{mpp}. Due to the high costs involved with energy processing systems, it is not uncommon to apply a reduction factor to the value of S_{max}^{j}. This procedure, which is believed to skew the results in favor of a higher active power curtailment, will, intentionally, be disregarded.

The figures 21, 22 and 23 exhibit maps of the locations, as well as sizings, of the PV systems obtained following the criteria of equation (24), for $S_P = 100\%$.

Figure 21 – PV system allocation map for the 34 Bus test case.

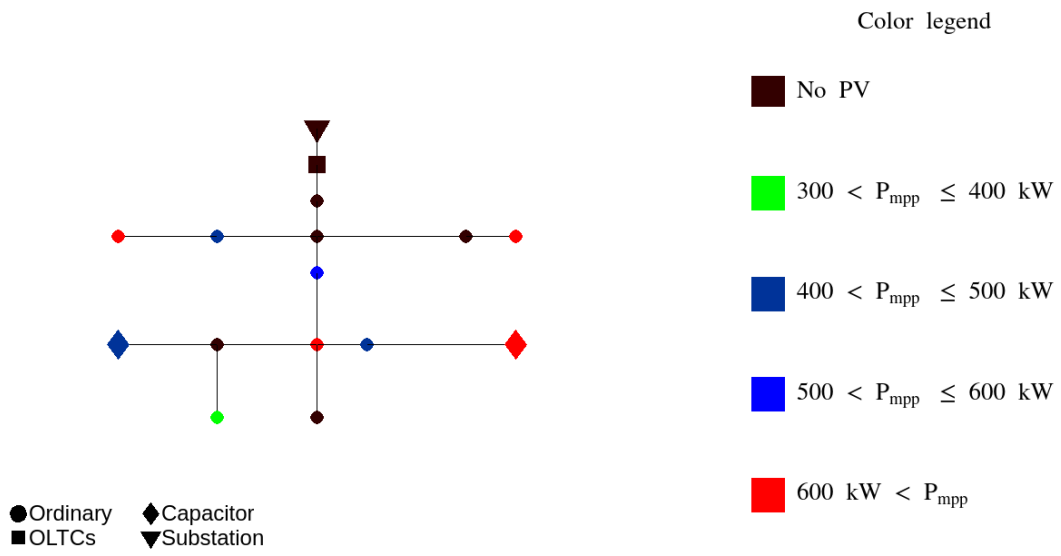

Source: The author.

Figure 22 – PV system allocation map for the 34 Bus test case.

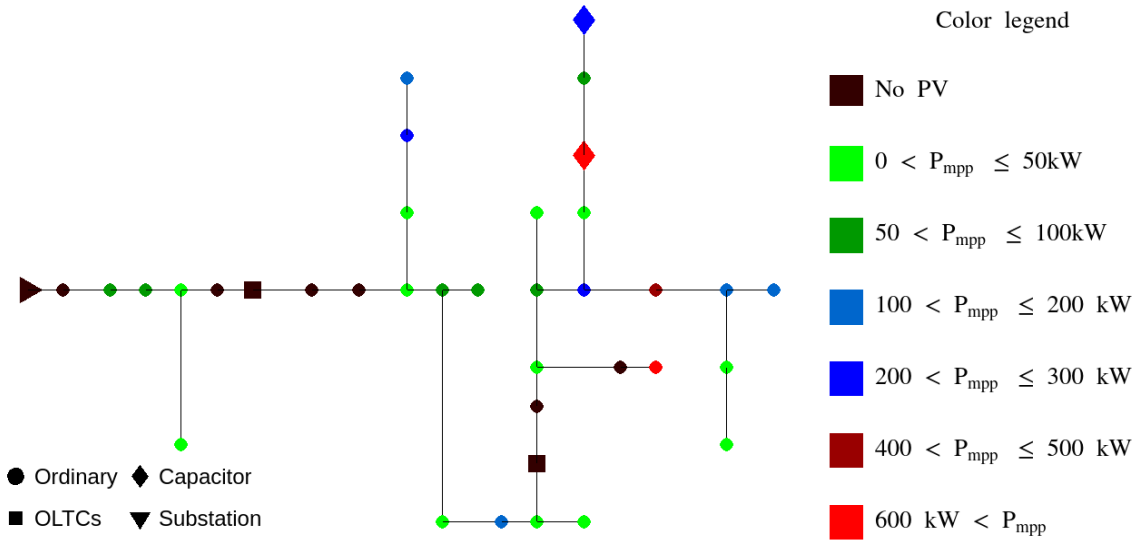

Source: The author.

Figure 23 – PV system allocation map for the 123 Bus test case.

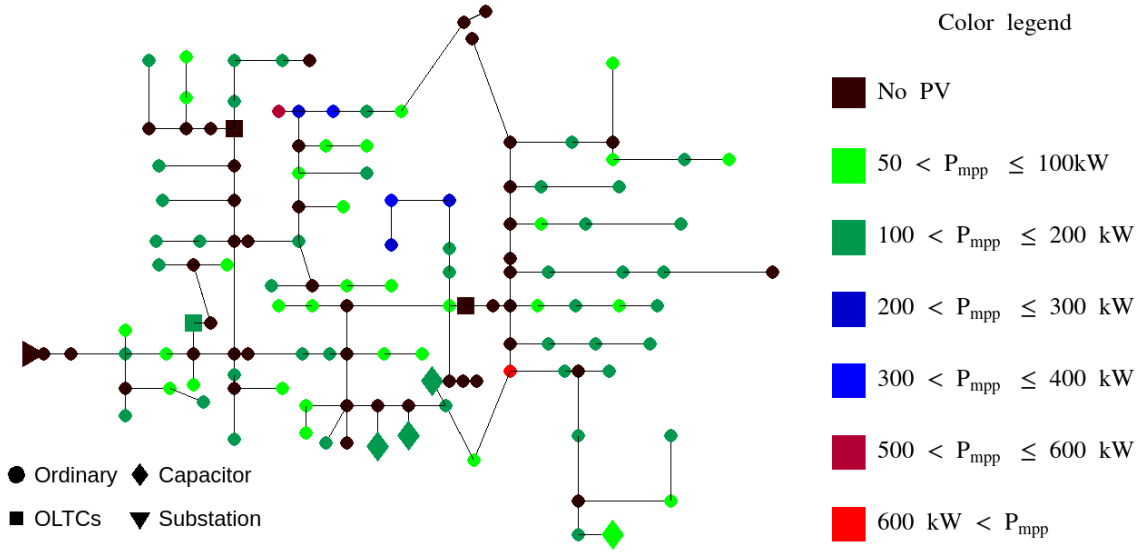

Source: The author.

As an attempt to isolate the effects of the tap changers in the curtailment of the PVs energy generation, the sequence of yearly simulations, as specified until now, was repeated twice. The first repetition was executed with all the tap changers of the three feeders deactivated, while, during the second, all of them were configured to operate normally.

The Volt-Var curve applied to all units, during all simulations, was fixed with a parametrization corresponding to the one shown in figure 24. Note that although category B DERs reactive power output functions may support a deadzone region, it is permissible, under the standard, to exclude it. Also, the variable $\bar{V}$ is the applicable voltage, calculated according to the standard specifications. The maximum reactive power absorption and generation limits were unrestricted, i.e, considered as the nameplate capability of each inverter.

Figure 24 – Configured Volt-Var characteristic curve during executed simulations.

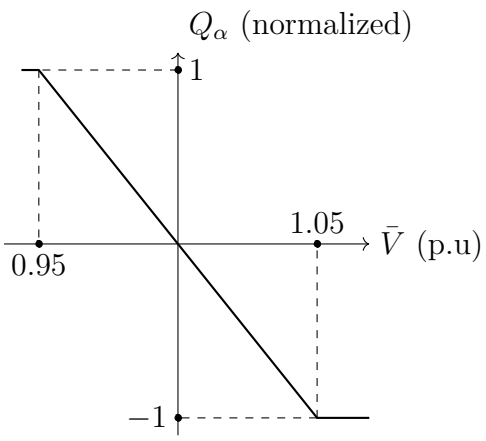

Source: The author.

During the simulations, the value of the energy extracted from each PV system, complying with reactive power prioritization, was calculated, alongside with the possible maximum energy that could be obtained if active power curtailment had not been imposed to it. Figure 25 illustrates how the setpoint of each one of the inverters would be adjusted in order to respect their capability curves following these two possibilities.

Figure 25 – Displacement of an inverter operation point when prioritizing active or reactive power.

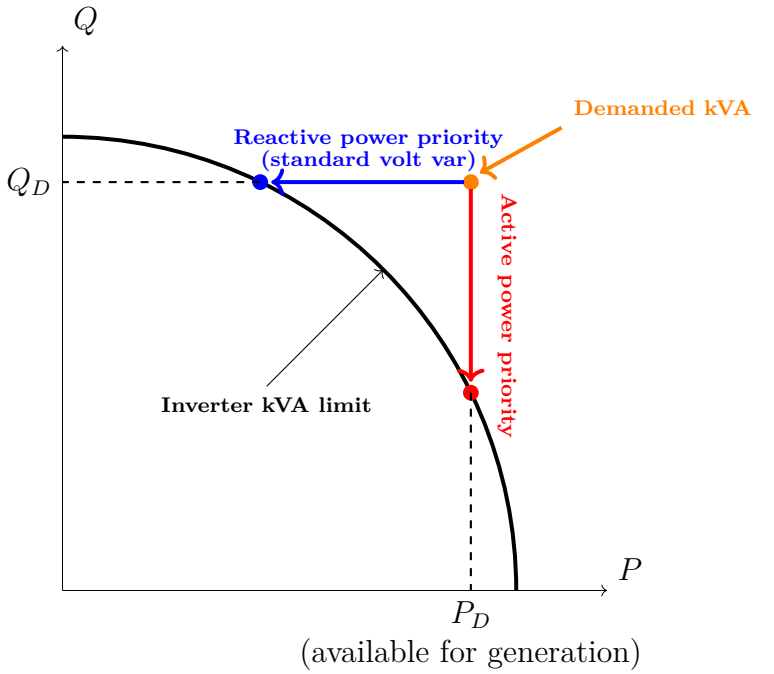

Source: The author.

Finally, table 5 shows a brief summary of the conditions imposed for the set of simulations. It is important to note that the PV scaling range condition, as exhibited in the table, is restricted to only 60% for the 34 Bus test case, because, due to the feeder characteristics, high levels of penetration would result in voltage profiles that, although may converge in a simulation, are not reasonable in an actual distribution feeder.

Table 5 – Simulation parameters. Each of the conditions presented were repeated for each feeder.

Simulation time	1 year
Stepsize	10 minutes
PV scaling (S_P) range	1 - 120%
PV systems inclination azimuth	180° (facing south)
PV systems inclination slope	33.07°

Source: The author.

4 RESULTS

In order to better understand how the operation of tap changers may impact the curtailment of energy generation of photovoltaic energy resources, first, they were deactivated and, then, the proposed simulations were executed, for all the three feeders. The figure 26 exhibits the global curtailment as a function of the scaling percentage S_P, as defined in section 3.2, pertaining to the 13 Bus, 34 Bus and 123 Bus test cases.

Figure 26 – Global ratio of generation reduction (curtailment) as a function of the scaling percentage S_P.

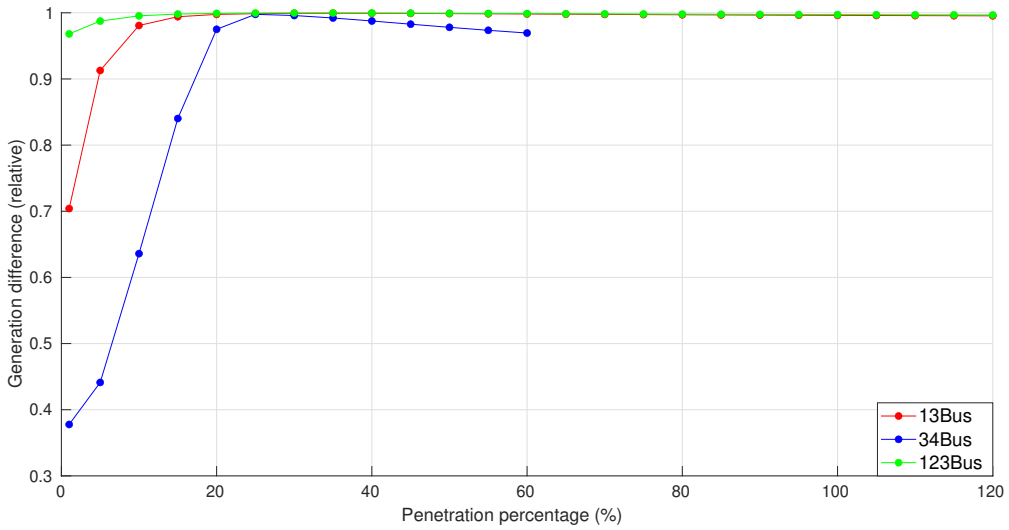

Source: The author.

Starting from the left side of the axis, in figure 26, there is an increase in the relative generation (i.e, a reduction of curtailment) until a point where it starts to decrease (i.e, the relative curtailment increases). Although this decrease may not be clearly visible for the 13 Bus and 123 Bus test cases, it can be easily noted for the blue curve, corresponding to the 34 Bus feeder.

The reason for the mentioned behavior of these curves suggests that there is an optimal scaling percentage S_P in which the relative curtailment is minimal. One relevant question related to this scaling point is if the voltages of the nodes of the feeders are also better regulated, or, in other words, if this point is also a point of minimum global voltage deviation. In order to answer this question, the metric specified in equation (26) was used:

$$M = \sum_{n=0}^{N} \sum_{i \in B} |V_i - 1| \tag{26}$$

where B is the set of all nodes belonging to each one of the feeders, and N, the number of timesteps which the PV units operated during each yearly simulation. This metric was calculated for each value of S_P, and the results are exhibited, for each one of the studied power systems, in figure 27. It is important to note that, in order to ease the visualization of the three curves, each one of them was normalized.

Figure 27 – 1-norm of the voltage deviations from 1 p.u with deactivated tap changers. For each curve, the results were also normalized.

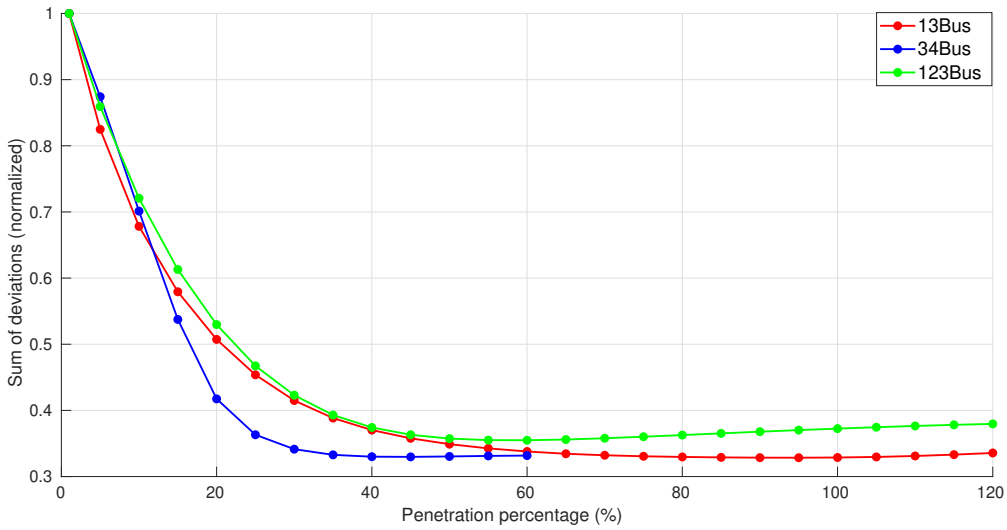

Source: The author.

Comparing each one of the curves in figure 26 with its respective counterpart in figure 27, it is possible to conclude that there is a significant displacement between the values of S_P which leads to minimum curtailments with their counterparts that result in the best voltage regulation, according to the criteria of equation (26). This displacement can be explained by comparing, *during the day*, the regulation of the feeders under the two scenarios. The figures 28, 29 and 30 exhibit a series of boxplots, for each one of the hours of the day through the year when solar irradiation was present, of the phase-neutral voltages pertaining to, respectively, the 13 Bus, 34 Bus and 123 Bus test cases, considering each one of the two mentioned critical points of S_P.

Figure 28 – Boxplot of the voltages, during each hour of the day, for the 13 Bus test case. The red boxes pertain to the point of best curtailment, while the blue ones, to the point of best overall regulation.

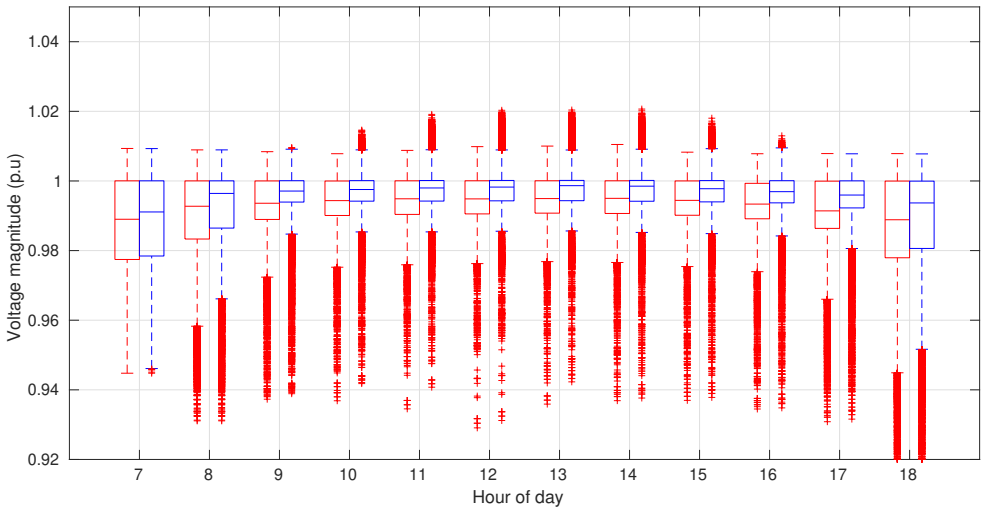

Source: The author.

Figure 29 – Boxplot of the voltages, during each hour of the day, for the 34 Bus test case. The red boxes pertain to the point of best curtailment, while the blue ones, to the point of best overall regulation.

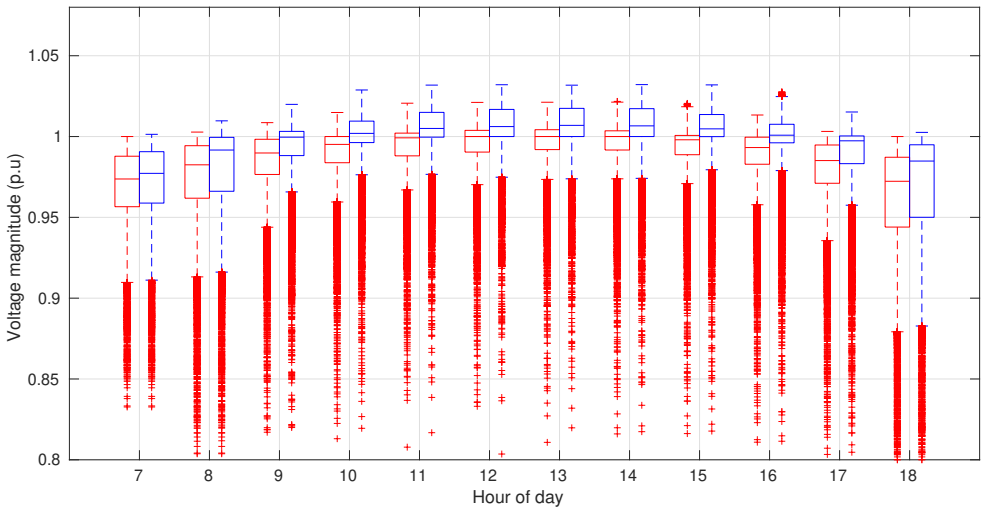

Source: The author.

Figure 30 – Boxplot of the voltages, during each hour of the day, for the 123 Bus test case. The red boxes pertain to the point of best curtailment, while the blue ones, to the point of best overall regulation.

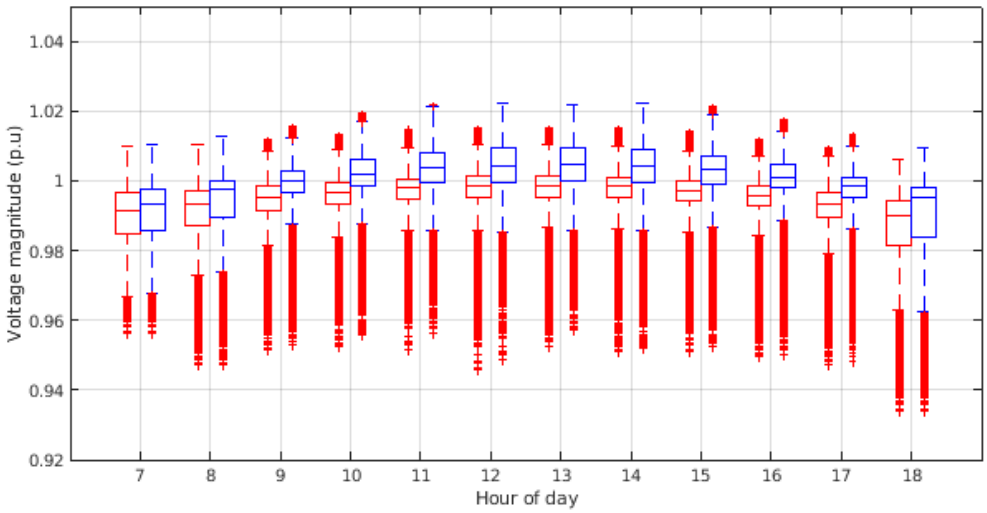

Source: The author.

Observing figures 28 and 30, it is possible to realize that, although the medians of the samples pertaining to the values of S_P that result in the best regulation (blue boxplots) are closer to one, there is a higher number of high-voltage outliers during peak generation hours. It is possible to infer, then, that the improved overall regulation is an effect achieved through a higher circulation of reactive power output, due to the volt-var performed by the inverters, during all hours of the day. The red boxes, related to the values of S_P with lower curtailment, present a less expressive number of outliers above 1 p.u, as well as a weaker tendency of overvoltages. Since this was possible with the lowest relative curtailment possible, the values of S_P which they are related to can be thought of

as the ones which, on a global sense, result in a better matching between the system loads and the generation units.

Until now, yet, it has not been discussed what are, specifically, the conditions of the feeders voltages when curtailment occurred. In order to investigate this issue, the figures 31, 32 and 33, which present a series of boxplots, hour by hour, pertaining to the feeders phase-neutral voltages, can provide useful insights. The red boxplots resulted from $S_P = 10\%$, while the blue ones, for the 13 Bus and 123 Bus test cases, from $S_P = 100\%$. Since this value of S_P was not simulated for the 34 Bus, the scaling percentage of 50% was used instead.

Figure 31 – Boxplots of the phase-neutral voltages pertaining to the 13 Bus test case and scaling percentages of 10% (red) and 100% (blue).

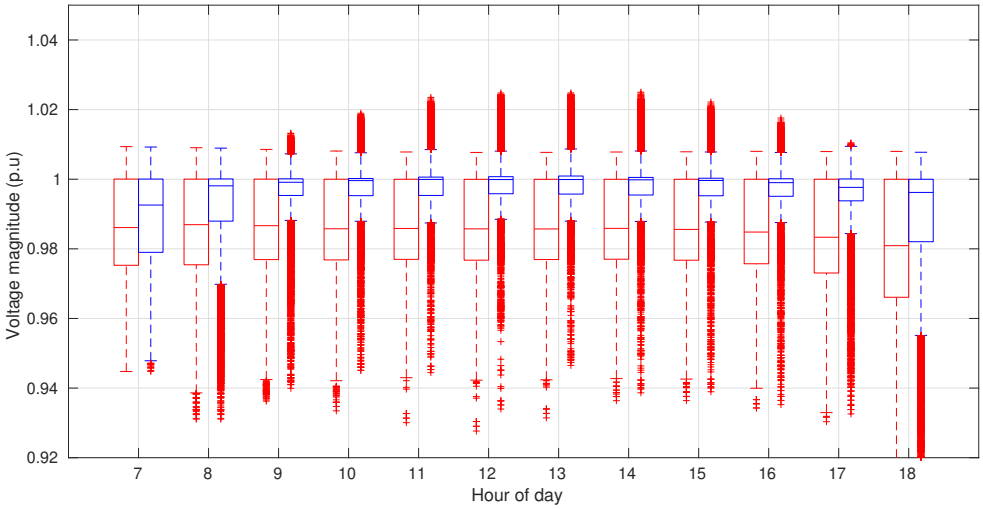

Source: The author.

Figure 32 – Boxplots of the phase-neutral voltages pertaining to the 34 Bus test case and scaling percentages of 10% (red) and 50% (blue).

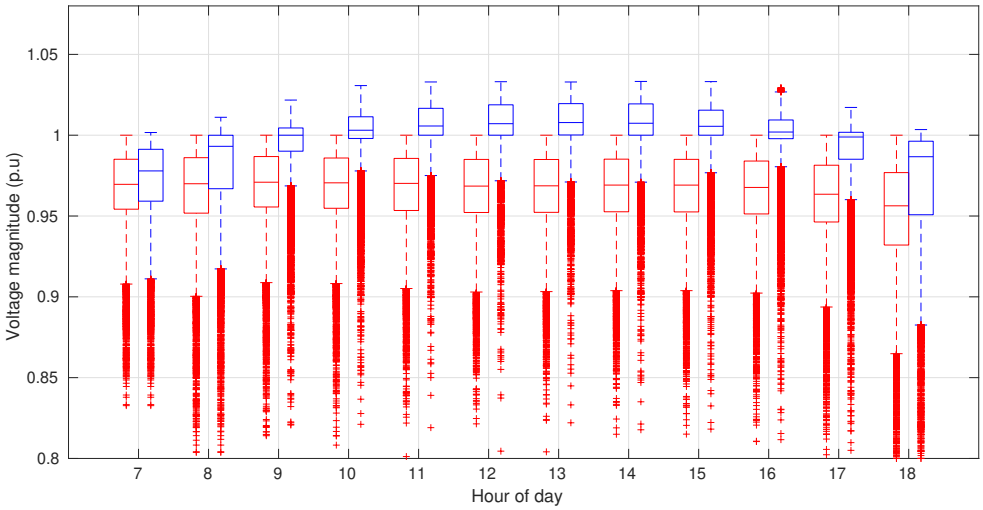

Source: The author.

Figure 33 – Boxplots of the phase-neutral voltages pertaining to the 123 Bus test case and scaling percentages of 10% (red) and 100% (blue).

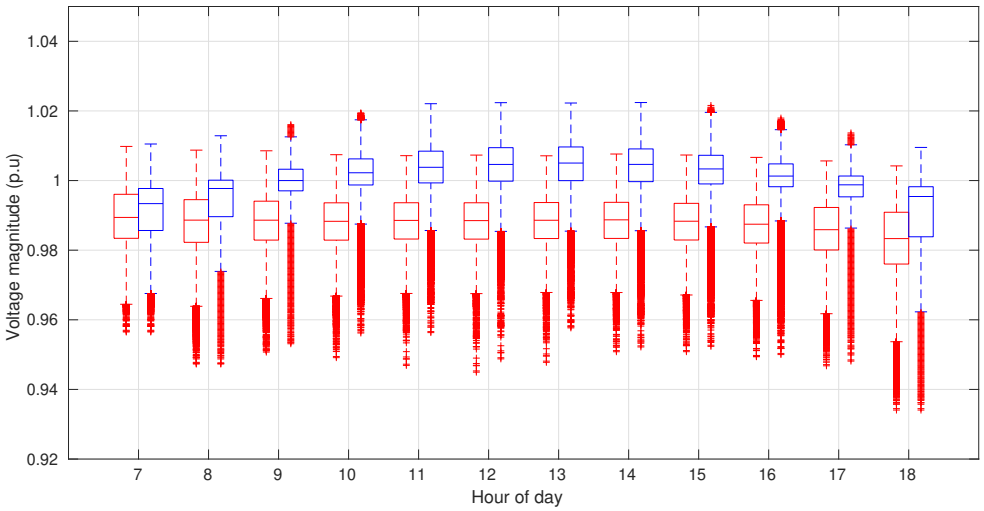

Source: The author.

It is important to make a few remarks about the previous figures. First, for $S_P = 10\%$, it is possible to observe that most of the feeders voltages have a high skewness towards below 1 p.u, while for $S_P = 100\%$ (or 50%, for the 34-Bus case), there is towards above 1 p.u. The main adverse effect of reverse power flow, pertaining to the frequency domain, is the undesired rise of voltages. Therefore, for the cases of $S_P = 10\%$, it is possible to infer that, during the majority of the hours, there was a requested effort from the inverter units to mitigate undervoltages that, although resulted in a reasonable reduction of generation, were not directly caused by the units active power injection. As the scaling increases, however, as can be seen in the blue boxplots corresponding to higher penetration levels of PVs, it is possible to relate the cause of the inverter units active power curtailment to the distributed generation.

The discussion of the previous paragraph suggests that, when the penetration level of photovoltaic systems is low, the cause of their efforts are linked more to normal feeder conditions, rather than the DERs themselves. The validity of this statement, however, is weakened as the penetration level increases.

Now, attention will be given to the differences between the curtailment curves of different feeders. According to figure 26, again, the 13 Bus and 123 Bus test cases presented, for high values of S_P, a very low overall curtailment. The curve of the 34 Bus, on the other hand, seems to quickly decline after its point of maximum. Also, for the same feeder, only points close to the point of minimum curtailment have a good ratio.

The 13 Bus and 123 Bus test cases are strong feeders, in which the $\frac{X}{R}$ ratio of its conductors tends to be higher than in comparison with the 34 Bus, composed of longer lines with worse expected volt-var efficiency. Hence, the higher amplitude of its curve is

attributed to, mainly, the phase characteristic of its impedances, although they may not be able to provide a complete explanation. For example, the low ratio of the 13 Bus, for low values of S_P, when compared with the 123 Bus, is an intriguing observation which could defy this reasoning.

The 13 Bus is known for being a (more) heavily loaded feeder than in comparison with the 123 Bus. As discussed previously, when the penetration of distributed generation resources is low, their efforts are mainly related to undervoltages mitigation, rather than the compensation of reverse power flow effects. Hence, a way to understand the differences, between the beginnings of these two feeders curtailment curves, is by comparing how much they are loaded.

An important remark regarding the discussion of the previous paragraph is that even strong feeders can present high curtailments when the penetration level of PVs is low, if they are heavily loaded. Such consideration must be taken in account when introducing DERs voltage support policies into a system.

The behavior of the curtailment through different seasons was also investigated. Figures 34, 35 and 36 depicts, again, the relative generation compared to the amount that could be produced if curtailment of active power did not occurred, but now separated between the four seasons of the year. It is worth noting that, for all the three figures, there is a tendency of higher curtailment during the winter when S_P is low. However, as its value increases, the highest reduction of generation occur during spring.

Figure 34 – Relative reduction of energy generation during the four seasons of the year pertaining to the IEEE 13-Bus test case.

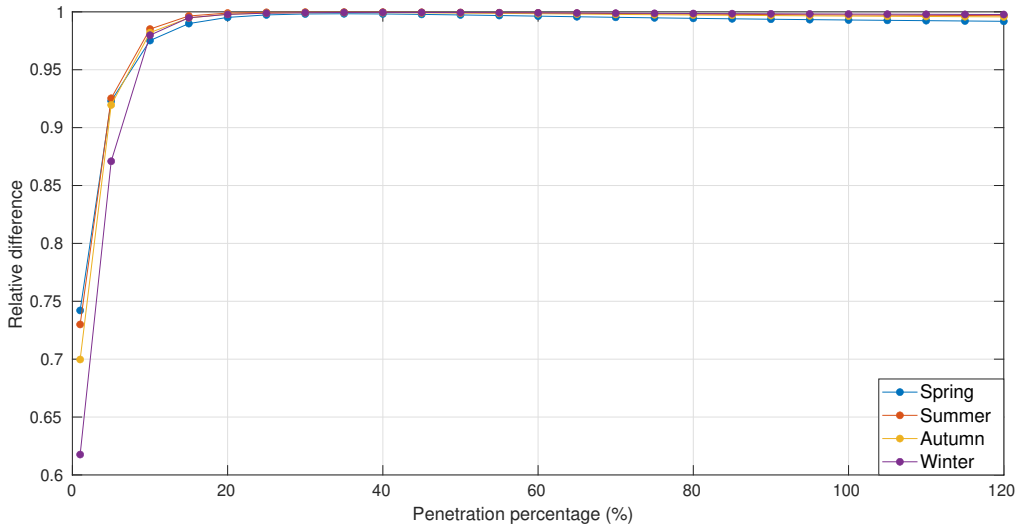

Source: The author.

When the penetration of PVs within a feeder is low, as discussed previously, there is a higher effort demanded from the inverter units employing volt-var to regulate undervoltages caused by the power demanded by the system loads. Due to the bad weather

Figure 35 – Relative reduction of energy generation during the four seasons of the year pertaining to the IEEE 34-Bus test case.

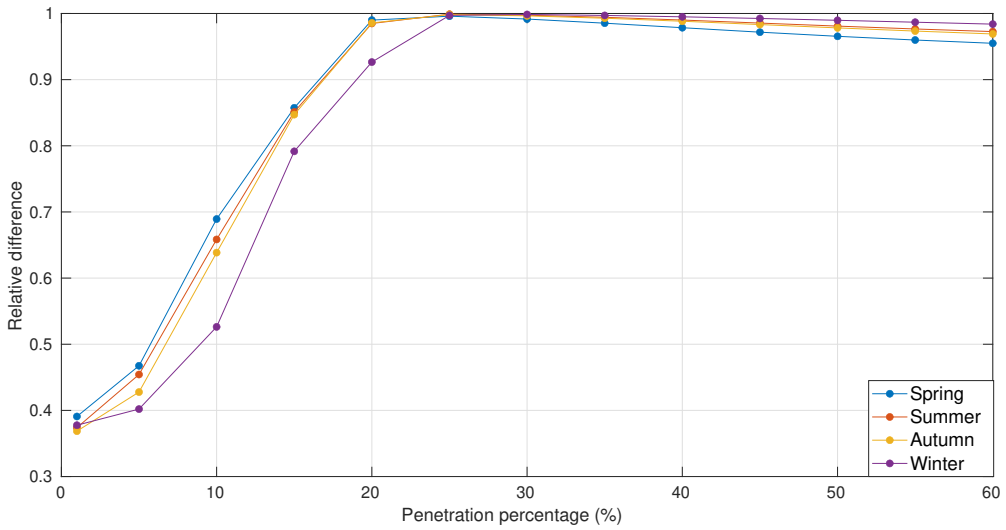

Source: The author.

Figure 36 – Relative reduction of energy generation during the four seasons of the year pertaining to the IEEE 123-Bus test case.

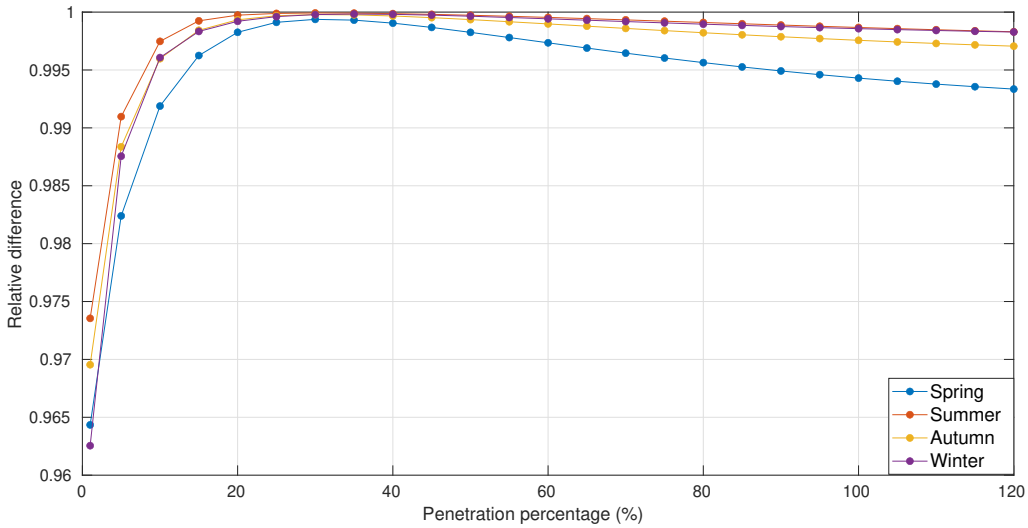

Source: The author.

of this season, the demand from the EPS is higher. This can be seen by visualizing the figure 20 of section 3.2, which exhibits the normalized load and PV timeseries together. Hence, in such conditions, the higher curtailment during winter can be explained as the result of an worsened system voltage regulation due to a stronger loading.

When it is spring, however, the situation is different. The peak consumption of the loads is lower, and there is a reasonable period in which the irradiation has high peaks. Thus, for high penetration levels of PVs, a higher curtailment should occur due to an increased effort, demanded from the inverters units, to mitigate the effects of an overall stronger reverse power flow.

An important topic to assess is related to how the curtailment vary between different buses within a feeder. In order to discuss this, the figures 37, 38, 39, 40, 41 and 42, which show the relative reduction of generation in the studied feeders, for the scaling percentages of 10 and 100 percent (10 and 50 percent, for the 34 Bus), were produced. A frequent trait present in the figures is that the buses located closer to the branches ends tends to present a higher curtailment than in comparison with the ones closer to the starts.

Figure 37 – Map of relative reduction of energy generation pertaining to the IEEE 13 Bus test case with $S_P = 10\%$

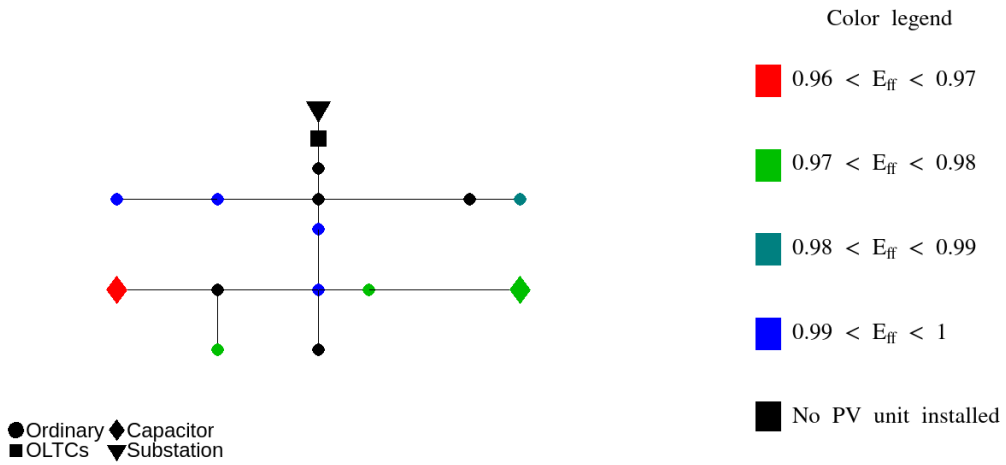

Source: The author.

Figure 38 – Map of relative reduction of energy generation pertaining to the IEEE 13 Bus test case with $S_P = 100\%$

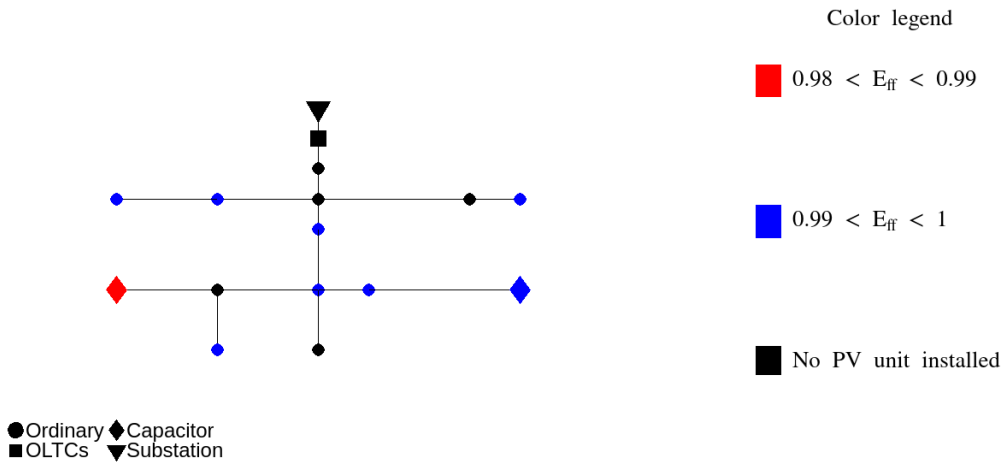

Source: The author.

Figure 39 – Map of relative reduction of energy generation pertaining to the IEEE 34 Bus test case with $S_P = 10\%$

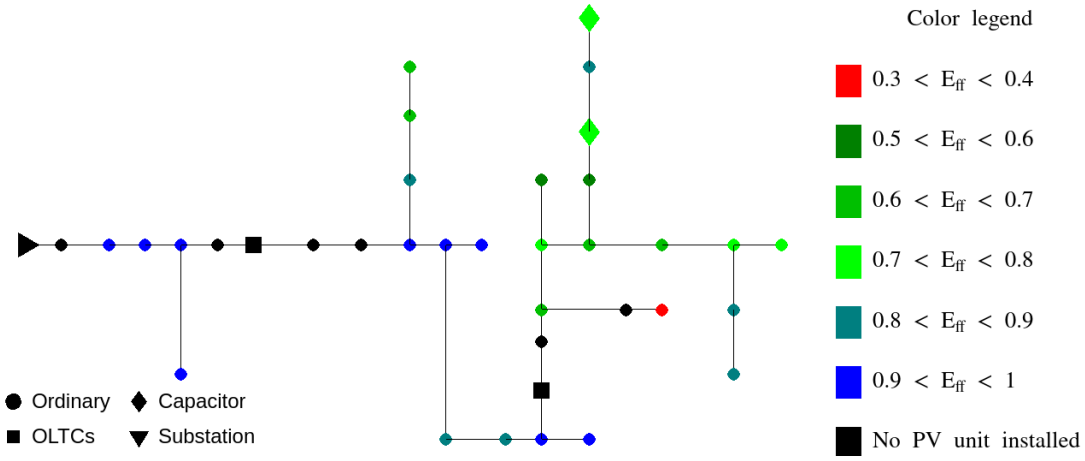

Source: The author.

Figure 40 – Map of relative reduction of energy generation pertaining to the IEEE 34 Bus test case with $S_P = 50\%$

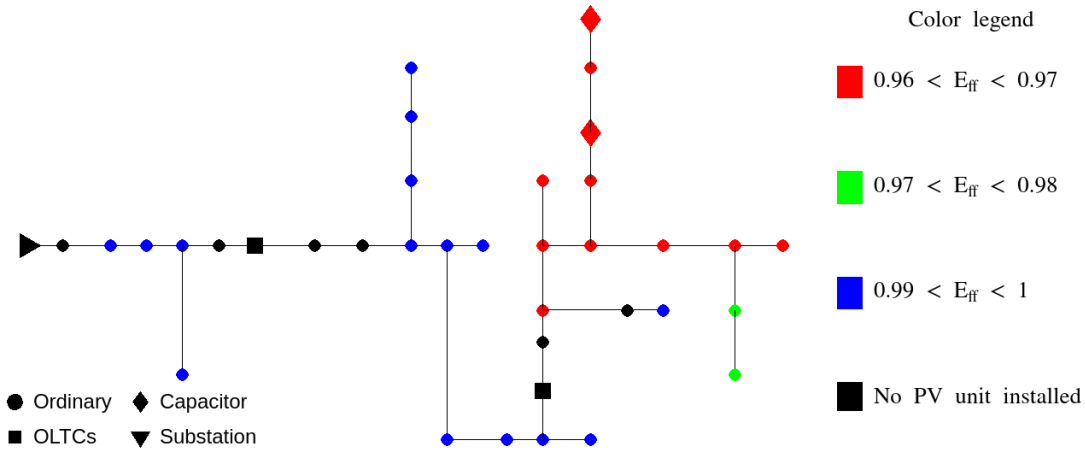

Source: The author.

Figure 41 – Map of relative reduction of energy generation pertaining to the IEEE 123 Bus test case with $S_P = 10\%$

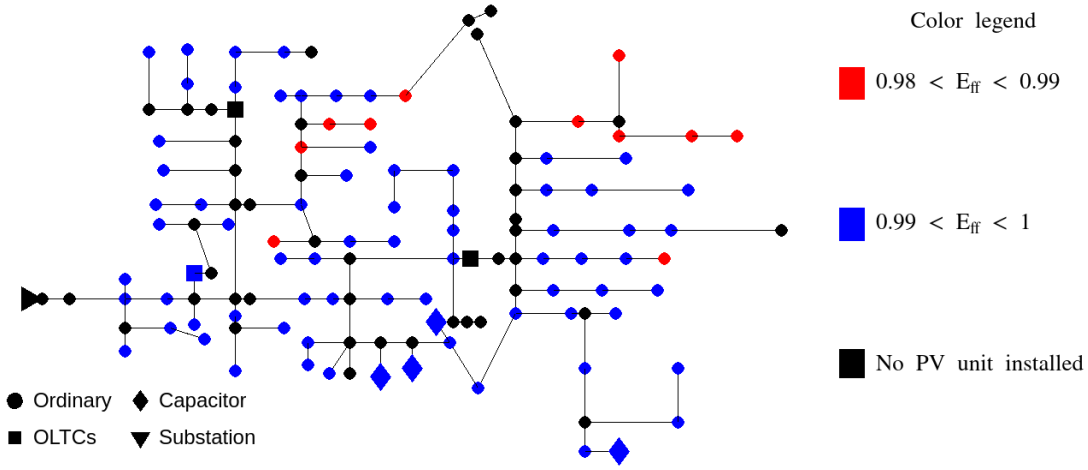

Source: The author.

Figure 42 – Map of relative reduction of energy generation pertaining to the IEEE 123 Bus test case with $S_P = 100\%$

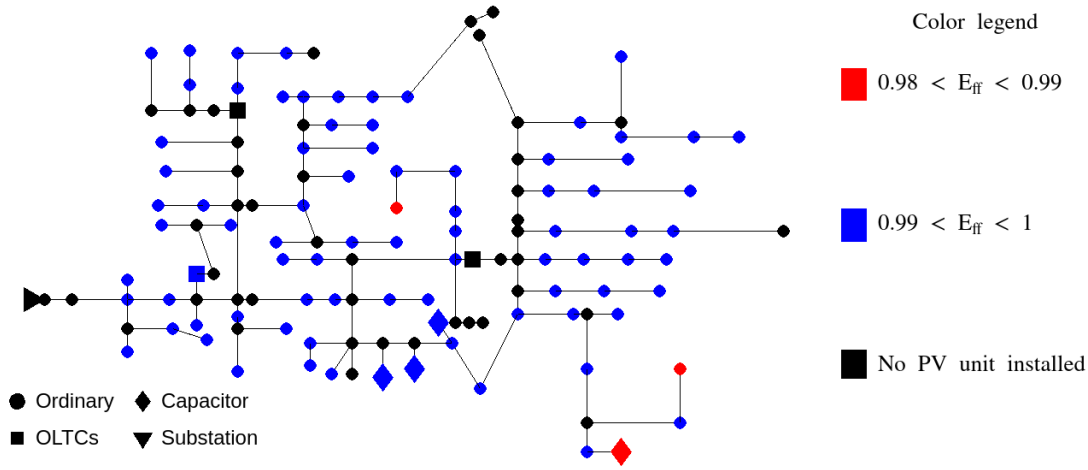

Source: The author.

It is important to remark, about the figures pertaining to low penetration levels ($S_P = 10\%$), that, on these cases, the main reasons of curtailment are the voltage regulation issues caused by the feeders own loads. One of the contributions of figures 37, 39 and 41 is that the impedances connecting these loads to its corresponding substations are also important when estimating the curtailment of active power from each PV.

Not necessarily a system located closer to the end of a feeder branch should have an worse curtailment. For the 13 Bus test case, for example, the inferior lateral branch on the left has two buses. The farthest of them possess a lower reduction than in comparison with the closest to the feeder main branch. This is believed to be an effect of the capacitor bank installed in the latter bus. Something similar can be observed for the 34 Bus test case also. Since undervoltages are to be expected when there are low penetration levels,

the use of capacitor banks should relieve the PVs inverters from having to contribute with voltage regulation. Thus, a fixed capacitor bank strategically allocated can improve not only the voltage profile of a region of a feeder, but also reduce the effort from DER units located nearby.

Interestingly enough, as can be seen in the figures 40 and 42, corresponding to the 34 Bus and 123 Bus test cases, when $S_P = 100\%$, even though it is expected that capacitor banks should negatively impact the curtailment of the units located close to them in such penetration level, the severity of this impact is low.

There is, for the 34 Bus test case, a particular branch (the latest, from left to right, connecting two buses) in which there is an improved curtailment, although there is not any capacitor bank installed along it. This particular case happened because the derived branch is a single-phase ramification of the most lightly loaded phase of the system. Hence, its buses should have a better regulation, if compared with the ones of the main branch close to the point of derivation, and, as a consequence, they present less curtailment.

Finally, the influence of the tap changers in the curtailment of active power of photovoltaic systems, demanded by the volt-var algorithm, will be evaluated. The same simulations on the three feeders were repeated, now with the tap changers reactivated and configured to setpoints of 1 per unit. The figure 43 depicts, under these conditions, the global curtailment curves as a function of S_P.

Figure 43 – Global ratio of generation reduction (curtailment) as a function of the scaling percentage S_P with tap changers considered.

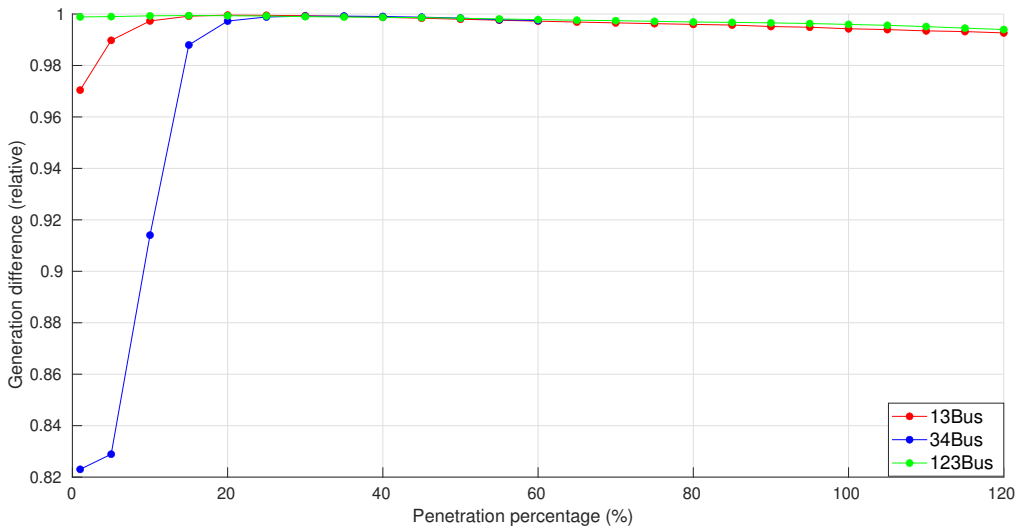

Source: The author.

It seems, when comparing figure 43 with figure 26, pertaining to the case without tap changers, that there is a significant improvement of the necessary overall curtailment for low values of S_P. According to the discussion until now, this was expected, because tap changers are effective in the mitigation of undervoltages within a section. However,

a different behavior can be observed for the 13 Bus and 123 Bus test cases when S_P is high. In order to understand what is behind these results, it is useful to visualize where, in each one of the feeders, the differences occured. Figures 44, 45, 46, 47, 48 and 49 depict the maps of curtailment for the three feeders, with the same scaling percentages as used previously when no tap changers were considered.

Figure 44 – Map of relative reduction of energy generation pertaining to the IEEE 13 Bus test case with $S_P = 10\%$ and tap changers activated.

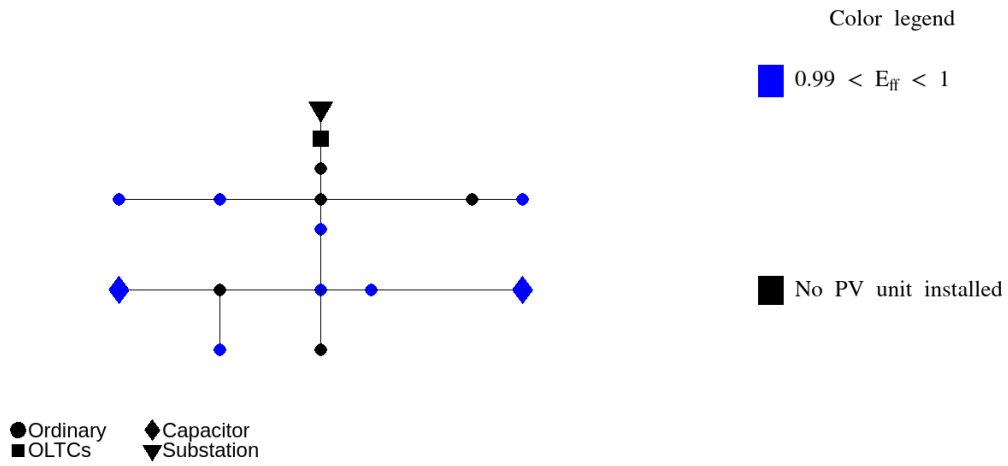

Source: The author.

Figure 45 – Map of relative reduction of energy generation pertaining to the IEEE 13 Bus test case with $S_P = 100\%$ and tap changers activated.

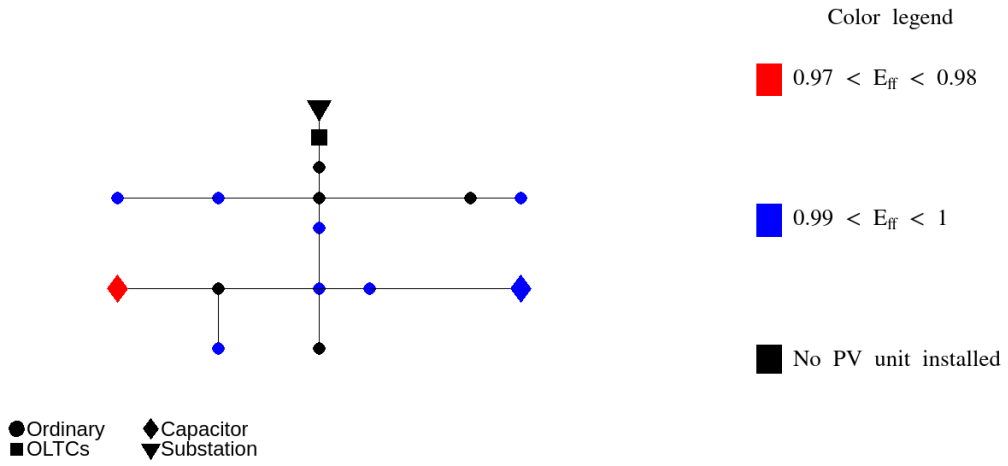

Source: The author.

Figure 46 – Map of relative reduction of energy generation pertaining to the IEEE 34 Bus test case with $S_P = 10\%$ and tap changers activated.

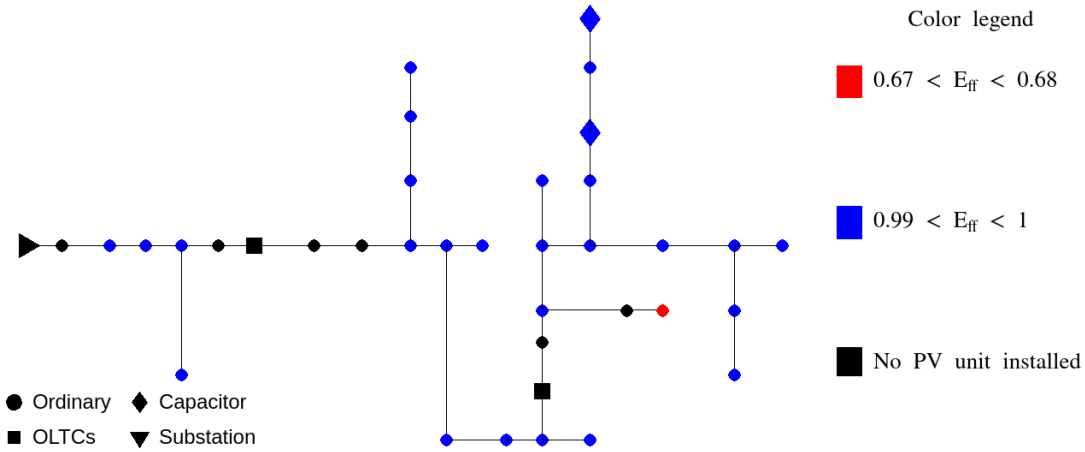

Source: The author.

Figure 47 – Map of relative reduction of energy generation pertaining to the IEEE 34 Bus test case with $S_P = 50\%$ and tap changers activated.

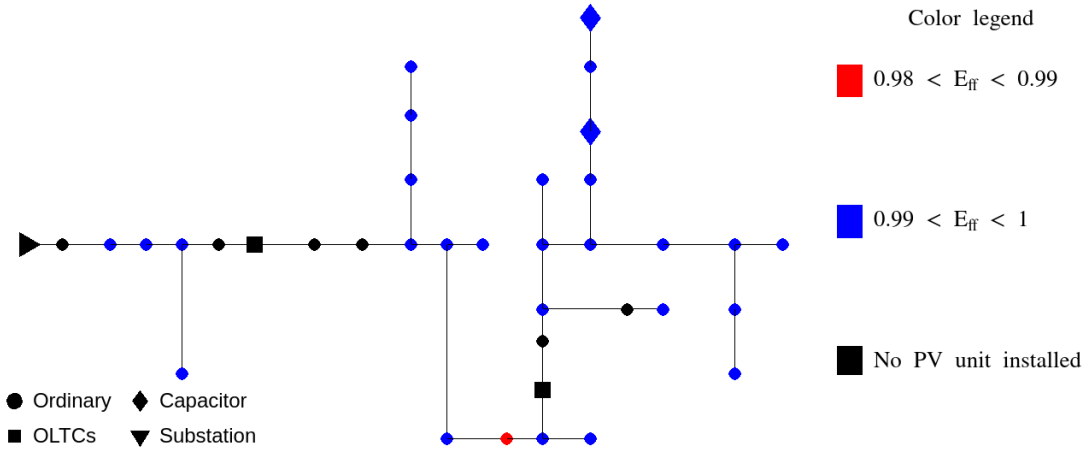

Source: The author.

Figure 48 – Map of relative reduction of energy generation pertaining to the IEEE 123 Bus test case with $S_P = 10\%$ and tap changers activated.

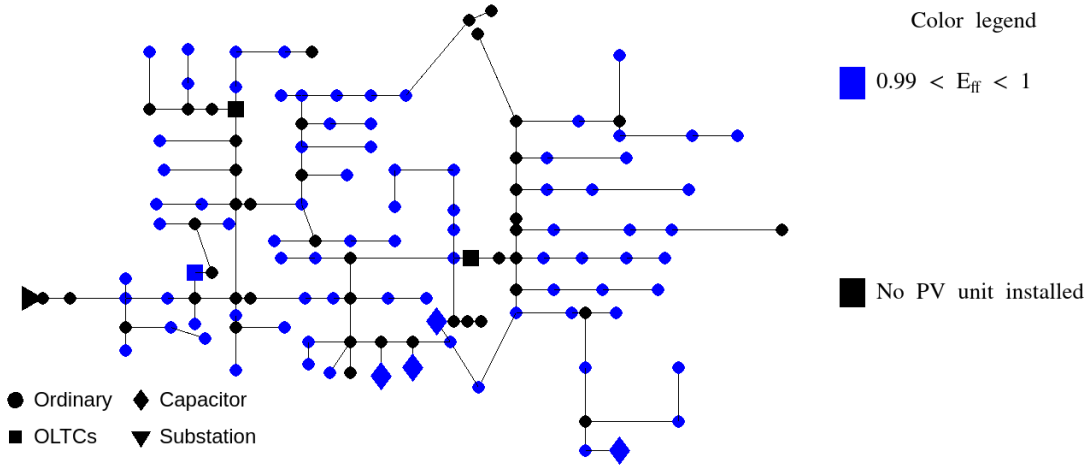

Source: The author.

Figure 49 – Map of relative reduction of energy generation pertaining to the IEEE 123 Bus test case with $S_P = 100\%$ and tap changers activated.

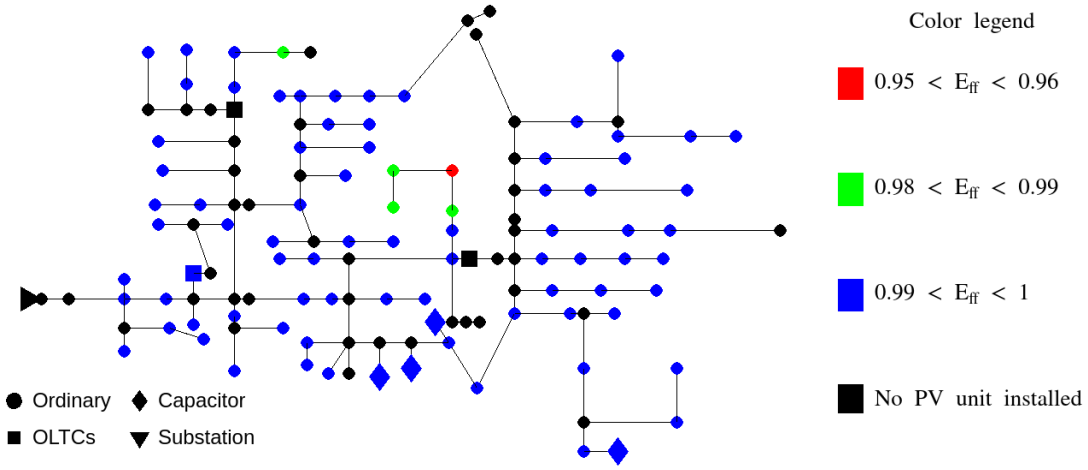

Source: The author.

When comparing figures 44, 46 and 48, corresponding to $S_P = 10\%$, with their respective counterparts without tap changers, it seems that there is either an improvement or no negative outcome in all buses of the three feeders. However, when $S_P = 100\%$, the figure 44, related to the 13 Bus, shows a deterioration in the improvement of the bus where the capacitor bank is installed. The figure 49, pertaining to the 123 Bus, also exhibits a branch, in the middle of the feeder, in which the same phenomenon occurred.

The two batches of simulations (with and without tap changers) were executed under the same conditions. Hence, the power demanded from the loads should be equal, as well as the available energy to be generated by the PVs. It is intriguing, them, why should the mentioned section, located in the middle of the system, contain buses with worse generation ratios.

If the necessary curtailment of the units located in buses after the tap changers is lower, then this should mean that the reactive power outputted by them, which contributed to improve not only their own local voltages, but also others from regions that are not primarily affected by the tap changers, is also lower. Not only that should be true, but also there is an increase in the severity of the reverse power flow in the regions which are not directly affected by the regulators, since the units mentioned previously are able to inject more active power into the grid and contribute less to voltage support. Hence, the observed deterioration of the curtailment must be related to an worsening of reliability caused by the reduction of the voltage support effort by the inverters installed in buses which are benefited by the tap changers operation.

5 CONCLUSIONS

In this work, it was proposed the study of the energy generation curtailment of photovoltaic systems due to employment of volt-var and the factors that may influence it. These tasks were carried out by considering sequences of full-year simulations of different feeders under varying conditions, i.e, with different penetration levels of PVs as well as with and without tap changers.

Several conclusions were inferred with the presentation of the results. First, the share of curtailment significantly varies with different levels of PVs penetration. Under the imposed scaling conditions, there is a certain percentage, for each feeder, in which the generation can be considered as better matching the demand from the loads, although it is displaced from the point where the photovoltaic systems and their inverters, operating with volt-var, can be considered as more beneficial to the grid. Also, the level of penetration impacts more the required curtailment in weak grids than in comparison with strong ones.

It was also identified that, when the penetration level of PV systems is low, the effort demanded from them is more significantly caused by the feeder own conditions, rather than the injection of active power by the units themselves. As the penetration level increases, however, the reverse power flow effects influence more the demand of voltage support from the systems inverters.

The $\frac{X}{R}$ ratio play an influential role in the curtailment itself, specially when the penetration level of PVs is high. The higher it is, the more efficient volt-var can be expected to be. However, this is not the only determining factor of the curtailment, since, when the capacity of the generation units is not high, the level of loading of the feeder should also be considered, as well as other locational factors which were identified.

Seasons also exert a strong influence on the overall curtailment. When the penetration level of the PVs is low, a higher curtailment should be expected during periods with higher load demand, while, when the level is high, a similar result should occur when there is a lower load demand.

Finally, tap changers of transformers also impact, in a significant degree, the curtailment behavior of a feeder, not only globally, but also locally. Although they mostly positively affected the curtailment of units within the considered feeders, it is possible that they induce a higher effort in units concentrated in specific sections whose voltages are not aided by their operations. Capacitor banks, on the other hand, resulted in a significant positive impact when the penetration level is low in the feeders studied, while the expected negative one for high levels of penetration was low, although not insignificant.

Until this point, it can also be concluded that it is important, within the existent economical restrictions, to find a way to overcome the curtailment of active power in weak feeders, since not only they are more susceptible to the curtailment, but also suffer more

from a poor energy distribution reliability.

BIBLIOGRAPHY

1 KERSTING, W. H. *Distribution System Modeling and Analysis 2nd ed.* New York, US: CRC Press, 2007.

2 BHATTACHARYYA, S.; MYRZIK, J. M. A.; KLING, W. L. Consequences of poor power quality - an overview. In: *2007 42nd International Universities Power Engineering Conference*. [S.l.: s.n.], 2007. p. 651–656.

3 TURIMAN, M. S. et al. Analysis of high penetration level of distributed generation at medium voltage levels of distribution networks. In: *2022 IEEE International Conference on Power Systems Technology (POWERCON)*. [S.l.: s.n.], 2022. p. 1–6.

4 BLASI, T. M. et al. Evaluation of the impacts of renewables sources and battery systems in distribution feeders with different penetration levels. In: *2019 IEEE PES Innovative Smart Grid Technologies Conference - Latin America (ISGT Latin America)*. [S.l.: s.n.], 2019. p. 1–6.

5 MINTER, Z. et al. A study of imbalance levels attributed to photovoltaic penetration in distribution systems. In: *2020 IEEE/PES Transmission and Distribution Conference and Exposition*. [S.l.: s.n.], 2020. p. 1–5.

6 BATAWY, S. A. E.; MORSI, W. G. On the impact of high penetration of rooftop solar photovoltaics on the aging of distribution transformers. *Canadian Journal of Electrical and Computer Engineering*, v. 40, n. 2, p. 93–100, 2017.

7 FOKUI, W. S. T.; SAULO, M.; NGOO, L. Investigating the impact of pv penetration on the distribution network: Case of nairobi north distribution network. In: *2021 IEEE PES/IAS PowerAfrica*. [S.l.: s.n.], 2021. p. 1–5.

8 IEEE Standard for Interconnection and Interoperability of Distributed Energy Resources with Associated Electric Power Systems Interfaces. *IEEE Std 1547-2018 (Revision of IEEE Std 1547-2003)*, p. 1–138, 2018.

9 AGRAWAL, A. et al. Performance of pv generation feedback controllers: Power factor versus volt-var control strategies. In: *2015 North American Power Symposium (NAPS)*. [S.l.: s.n.], 2015. p. 1–6.

10 RYLANDER, M. et al. Default volt-var inverter settings to improve distribution system performance. In: *2016 IEEE Power and Energy Society General Meeting (PESGM)*. [S.l.: s.n.], 2016. p. 1–5.

11 WANZELER, T. M. et al. Assessing the performance of smart inverter volt-watt and volt-var functions in distribution systems with high pv penetration. In: *2018 Simposio Brasileiro de Sistemas Eletricos (SBSE)*. [S.l.: s.n.], 2018. p. 1–6.

12 UEDA, Y. et al. Analysis results of output power loss due to the grid voltage rise in grid-connected photovoltaic power generation systems. *IEEE Transactions on Industrial Electronics*, v. 55, n. 7, p. 2744–2751, 2008.

13 MIYAMOTO, Y.; HAYASHI, Y. Evaluating improved generation efficiency: One year using residential pv voltage control with a clustered residential grid-interconnected pv. In: *2012 3rd IEEE PES Innovative Smart Grid Technologies Europe (ISGT Europe)*. [S.l.: s.n.], 2012. p. 1–8.

14 MOTURI, N.; ZILLMANN, M. Investigating the performance of inverter control modes in high solar pv penetration scenarios. In: *2021 IEEE PES Innovative Smart Grid Technologies - Asia (ISGT Asia)*. [S.l.: s.n.], 2021. p. 1–5.

15 PULFREY, D. L. *Photovoltaic Power Generation*. New York: Van Nostrand Reinhold Company, 1978.

16 KRAUTER, S. C. W. *Solar Electric Power Generation - Photovoltaic Energy Systems*. 1. ed. Berlin Heidelberg: Springer Berlin, Heidelberg, 2006.

17 AGHAMOLKI, H. G. et al. Moving to single-phase voltage regulation saves utility costs, improves power quality for industrials. In: *2020 IEEE/PES Transmission and Distribution Conference and Exposition (T&D)*. [S.l.: s.n.], 2020. p. 1–5.

18 MICHALSKY, J. J. The astronomical almanac's algorithm for approximate solar position (1950–2050). *Solar Energy*, v. 40, n. 3, p. 227–235, 1988. ISSN 0038-092X. Disponível em: <https://www.sciencedirect.com/science/article/pii/0038092X8890045X>.

19 KAMPHUIS, N. et al. Perspectives on the origin, derivation, meaning, and significance of the isotropic sky model. *Solar Energy*, v. 201, p. 8–12, 2020. ISSN 0038-092X. Disponível em: <https://www.sciencedirect.com/science/article/pii/S0038092X20301948>.

20 PEREZ, R.; SEALS, R.; MICHALSKY, J. All-weather model for sky luminance distribution—preliminary configuration and validation. *Solar Energy*, v. 50, n. 3, p. 235–245, 1993. ISSN 0038-092X. Disponível em: <https://www.sciencedirect.com/science/article/pii/0038092X9390017I>.

21 DUFFIE WILLIAM A. BECKMAN, N. B. J. A. *Solar Engineering of Thermal Processes, Photovoltaics and Wind*. 5. ed. Hoboken, New Jersey: John Wiley & Sons, Inc, 2020.

22 GHOSH, G. L. A. *Power Quality Enhancement Using Custom Power Devices*. 1. ed. Massachusetts, USA: Kluwer Academic Publishers, 2002.

23 HART, D. W. *Power Electronics 1st Edition*. [S.l.]: McGraw Hill, 2011.

24 MOHAN TORE M. UNDELAND, W. P. R. N. *Power Electronics Converters, Applications and Design 3nd. edition*. United States of America: John Wiley and Sons, Inc, 2003.

25 SCHNEIDER, K. P. et al. Analytic considerations and design basis for the ieee distribution test feeders. *IEEE Transactions on Power Systems*, v. 33, n. 3, p. 3181–3188, 2018.

26 SENGUPTA, M. et al. The national solar radiation data base (nsrdb). *Renewable and Sustainable Energy Reviews*, v. 89, p. 51–60, 2018. ISSN 1364-0321. Disponível em: <https://www.sciencedirect.com/science/article/pii/S136403211830087X>.

A ANISOTROPIC SKY MODELS

The isotropic sky model, as mentioned in chapter 2, is the most widely used, due to its simplicity in the calculation of irradiance transposed to a photovoltaic panel plane. However, it fails to realistically represent the distribution of scattered solar irradiation. This appendix aims to provide an understanding of the differences between the anisotropic and isotropic sky models, with emphasis on the model presented in [20].

Recalling equation (19), presented in section 2.6 to calculate the contribution of DHI according to the isotropic sky model, the factor

$$V_F = \frac{1 + \cos(\beta)}{2} \tag{27}$$

is named the view factor, which can be interpreted as a geometrical transposition factor, to the panel plane, of the uniformly scattered portion of DHI. Solar irradiance, however, does not arrive equally from all directions. Closer to the sun beams, there is a higher concentration of irradiation than in comparison with far. This means that it is more reasonable to divide DHI into two components: the circumsolar and a (reduced) isotropic. Equation (19), then, can be modified into equation (28) to reflect these considerations:

$$Irrad_{DHI} = (1 - F_1)\left(\frac{1 + \cos(\beta)}{2}\right) + F_1 \frac{\cos(\beta)}{\cos(\theta_S)} \tag{28}$$

where the factor F_1 represents the fraction of DHI that is circumsolar.

In the model actually used in this work, a further step is taken in the characterization of the diffuse irradiance. By definition, i.e, the way it is measured, the value of DHI pertains to an horizontally-inclined surface. However, there is also a third component of DHI that arrives from the far distant horizon. Ideally, this irradiance should reach the region of interest close to being parallel with the surface, and, hence, should be superposed to equation (28) when considering tilted surfaces, resulting in equation (29). Note that the extra term is simply the orthogonal projection of the mentioned irradiance in direction of the considered panel.

$$Irrad_{DHI} = (1 - F_1)\left(\frac{1 + \cos(\beta)}{2}\right) + F_1 \frac{\cos(\beta)}{\cos(\theta_S)} + F_2 \sin(\beta) \tag{29}$$

Equation (29) is the equation used to transpose the diffuse horizontal irradiance to inclined surfaces (actually, the second term is usually slightly corrected to avoid numerical issues when θ_S is close to 90°). However, there is an issue when considering the use of it. Until now, it is unclear how to properly choose the factors F_1 and F_2.

The quantity defined as

$$\epsilon = \frac{DHI + \dfrac{DNI}{\cos(\theta_S)} + 5.535 \cdot 10^{-6} \cdot {\theta_S}^3}{1 + 5.535 \cdot 10^{-6} \cdot {\theta_S}^3} \tag{30}$$

is the clearness index, a measure of how clear a sky condition is. Based on this value, it is possible to obtain six auxiliary coefficients which relate, linearly, the parameters F_1 and F_2, separately, to the solar zenith angle, the clearness index and a third variable known as the brightness parameter:

$$\Delta = m\frac{DHI}{G} \tag{31}$$

Finally, with the factors F_1 and F_2 in hand, it is possible to use equation (29).

Equations from anisotropic sky models are known for better matching experimental data, since the isotropic model tends to, in a consistent manner, result in lower values of transposed irradiance. Figure 50 exhibits a comparison between the irradiation timeseries used in this work, and the one that would result if an isotropic sky model were assumed. As can be seen in it, the previous statements agree with the figure.

Figure 50 – Irradiance time-series calculated using the anisotropic and isotropic sky models for the numerically determined tilt angle.

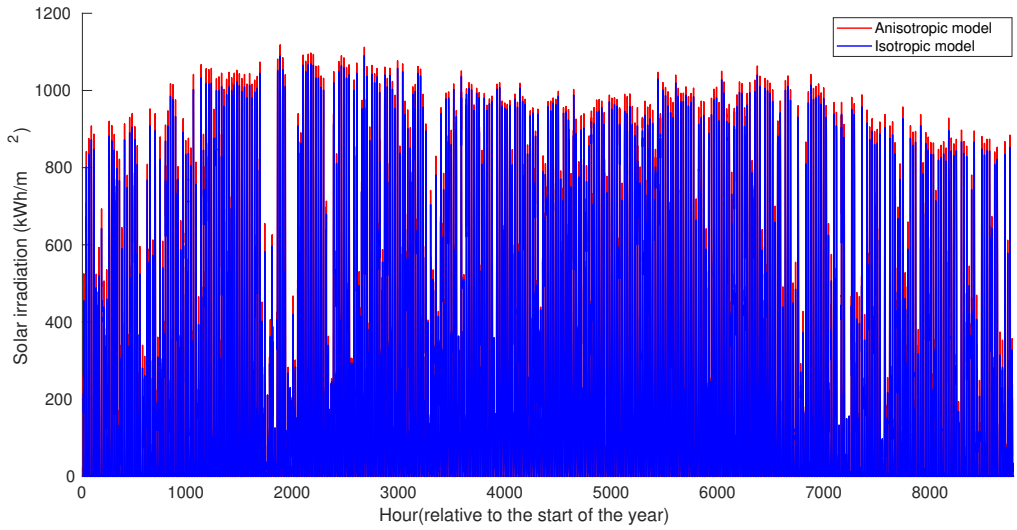

Source: The author.

The differences between the values calculated using the anisotropic and isotropic sky models, in this case, are small. Figure 51 depicts the same comparison, but considering the tilt angle determined according to the practical rule instead ($\beta = 40.7°$) instead.

Figure 51 – Irradiance time-series calculated with the anisotropic and isotropic sky models for the practical rule tilt angle.

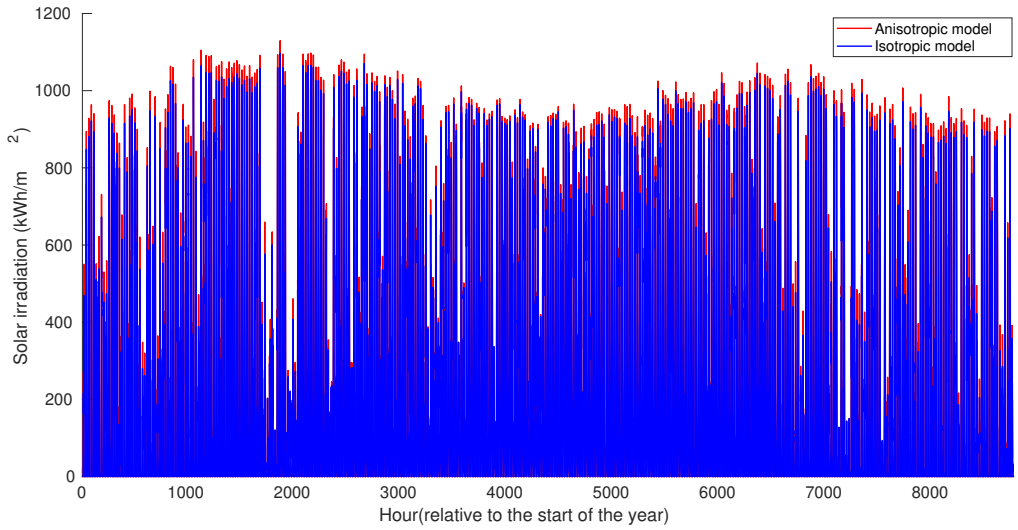

Source: The author.